2023-02-05

Estimate of uncertain cohesive suspended sediment deposition rate from uncertain floc size in Meghna estuary, Bangladesh

Sarwar, S

10.1016/j.ecss.2022.108183
Estuarine, Coastal and Shelf Science
Elsevier BV

Estimate of uncertain cohesive suspended sediment deposition rate from uncertain floc size in Meghna estuary, Bangladesh

Sifat Sarwar[a,b,*], Alistair G.L. Borthwick[c,d]

[a]Institute for Energy Systems, School of Engineering, The University of Edinburgh, The King's Building, Edinburgh, UK, EH9 3DW

[b] Architecture Discipline, Science, Engineering and Technology School, Khulna University, Khulna 9208, Bangladesh

[c]Institute for Infrastructure and Environment, School of Engineering, The University of Edinburgh, The King's Building, Edinburgh, UK, EH9 3JL

[d]School of Engineering, Computing and Mathematics, University of Plymouth, Drake Circus, Plymouth, PL4 8AA, UK[1]

*Corresponding author:

Sifat Sarwar

Architecture Discipline, Science, Engineering and Technology School,

Khulna University, Khulna 9208, Bangladesh

Email: sifatsarwar@arch.ku.ac.bd

Tel: +880 1321 571519

Highlights

- Uncertainty in sedimentation rate in the Meghna estuary is substantial.
- Numerical derived distribution approach gives rapid estimate of uncertainty.
- Suspended sediment erosion/deposition is strongly linked to local flow speed.
- Flocs deposit in areas where the current speed approaches zero.

[1] Present address: Architecture Discipline, Science, Engineering and Technology School, Khulna University, Khulna 9208, Bangladesh

ABSTRACT

Suspended sediment in the Meghna estuary, Bangladesh, typically consists of fine to medium silt near the water surface, silty sand at increasing depth, and sandy silt close to the bed. The behavior of fine, cohesive sediment in a complex environment with multiple drivers, such as river and tidal flows, is comparatively little understood because the deposition and erosion processes depend on many chemical, biological, and physical factors. This article examines the propagation of uncertainty from input floc size to output sedimentation rate in the Meghna estuary, Bangladesh, using a fine-sediment hydro-morphodynamic model that utilizes the cohesive sediment transport module in Delft3D. We assume that sediment particles and flocs are both single-sized throughout the solution domain. The effect of uncertainty in floc size on output sediment transport statistics is examined at three sites of interest located in the Meghna estuary using a novel numerical derived distribution approach. After deriving the probability distribution of suspended cohesive sediment, we find the coefficient of variation to range from 20% to 38% across the three locations. Planners therefore need to consider substantial uncertainty in cohesive sediment transport estimates for the coastal zone of Bangladesh, especially given the increased risk of flooding in deposition-prone areas as they become shallower. The methodology may be readily extended to the estimation of uncertainty in land reclamation and erosion control planning studies.

Keywords: Cohesive suspended sediment, floc size, Meghna estuary, uncertainty, sediment deposition rate

1 Introduction

The Bengal Basin, also known as the Ganges-Brahmaputra-Meghna Basin, consists of Bangladesh and parts of three eastern states of India (West Bengal, Assam and Tripura). According to Siddique-E-Akbor et al. (2011), more than 90% of the river flow passing through Bangladesh originates in upstream countries such as India and Nepal, whereas Bangladesh occupies only 7% of the total Ganges-Brahmaputra-Meghna basin area. The riverine discharge through the Meghna estuary is the fourth largest in the world (Milliman and Meade, 1983; Mukherjee et al., 2009), and the sediment discharge rate of $\sim 1 \times 10^9$ t/yr is the highest (Goodbred and Kuehl, 2000a; Mukherjee et al., 2009). 30%

of the sediment flux is deposited on floodplains, 40% in the marine area, and 10% in the Sundarbans and active Bengal delta, with the remaining 20% washed into the Bay of Bengal (Goodbred and Kuehl, 1999; Rogers et al., 2013, Seijger et al., 2019).

The Meghna estuary covers the zone of transformation of the Meghna River as it flows to the Bay of Bengal over a shallow shelf to a deeper basin. Several channels have formed in the estuary and they carry the river discharge to the bay. Large islands such as Bhola, Hatia, and Sandwip are located at the mouth of the estuary. According to Jacobsen et al. (2002), the Meghna Estuary is a 'Coastal Plain' estuary, implying that the estuary is very sensitive to its drivers, including tidal conditions, river discharge, and wind speed (Fischer et al. 1979). Local hydrodynamic conditions dominate sediment transport in the Meghna estuary, affecting grain size distribution, suspended sediment concentration, bed composition, and morphology. Sediment moves back and forth in the estuary, because monsoon river discharges bring sediment downstream to the estuary whereas the daily tidal prism pushes sediment back upstream (i.e. inland) through tidal channels (Barua et al., 1994; Goodbred and Kuehl, 2000b; Rogers et al., 2013; Seijger et al., 2019). Fig. 1 shows the elevation of the Bengal basin, which mainly comprises flat land of altitude about 5-10 m above mean sea level.

Bangladesh's distinct monsoon and dry seasons produce correspondingly different magnitudes of rainfall, river flow, and sediment yield throughout the year. During the monsoon season, rainfall is very intense and consequently the river flow greatly increases. Heavy rainfall in the Himalaya region raises the sediment yield of its constituent rivers. The combined effect of flow and sediment dominates the characteristics of the rivers, and hence the character of the Meghna estuary, where complex interactions also take place between river and tide (Akter et al., 2016). Erosion and deposition of sediment depend on local currents in the river and estuary; in fast currents there is sufficient shear to erode the bed with sediment particles transported predominantly in suspension (Brammer, 2014). The banks and bed level of the Meghna estuary have changed almost continuously over the centuries, with extensive erosion and deposition occurring near the islands. River erosion is a perennial problem in Bangladesh, which contains a network of about 230 rivers. The scarcity of land exposes residents living in the high-risk zone to natural disasters.

In the 1960s, extensive embankment construction commenced in the coastal area of Bangladesh. The works provided flood protection by decreasing land submergence and prohibited sediment from reaching the delta front by reducing sediment input to the delta. Dikes substantially

altered the hydro-morphodynamic characteristics of the delta by raising water levels in the diked channels and reducing sediment input, which in turn enhanced changes to the local erosion-accretion pattern in the channels (Mikhalov and Dotsenko, 2007). By considering a map overlay of shoreline position from the Lloyd's survey in 1840 and the LANDSAT image in 1984, Allison (1998*)* (cited by Mikhailov and Dotsenko, 2007), observed that significant land erosion and accretion occurred near the mouth of the Meghna Estuary during the intervening time. Allison (1998) calculated the volume of eroded and accreted land at various locations from different maps over several time periods and found a trend of net sediment accumulation at the delta front. With the help of satellite images, Mahmood et al. (2020) produced a shoreline movement map for 1980-2016 that demonstrates the entire mouth of the Meghna estuary is geographically very dynamic.

Erosion and accretion processes have been transferring sediment around Bhola, Sandwip, and Hatia islands. Barua (1997) reported that the erosion rate at the northeast bank boundary of Bhola had an average value of about 150 m per year between 1940 and 1963. Using LANDSAT satellite images from 1989 to 2018, Anwar and Rahman (2021) found that the northeast face of Bhola had a shore erosion rate of 139 m/year, and the southeast part of the island experienced a shore erosion rate of 40 m/year. Brammer (2014) compared land boundaries between 1984 and 2007, finding that about 40% of the eastern side of Sandwip island had been eroded, though there was a net accretion of 451 km^2 in the Meghna estuary. Considerable erosion and accretion occurred simultaneously at Hatiya island, another dynamic island in the Meghna estuary, with maximum shoreline shift rates of 138.5 m/year seaward and 285.4 m/year landward (Kabir et al., 2020). Kabir et al. also observed that the tidal flats around this island are very active, and predominantly accreting sediment. To the west of the estuary, the Sundarbans area is accretion prone, with the bed level increasing with rising sea level because of sediment deposition (Rogers et al., 2013). In recent years, Bomer et al. (2020) investigated bed surface elevation change and sediment accretion near the Sundarbans for the years 2014-2019, and confirmed that bed elevation rise is occurring, with the rate of elevation gain exceeding the rate of relative sea level rise. Active land formation is also evident at newly formed land (locally named "Char") in the riverine and coastal areas (Sarker et al., 2003).

The bed of the Meghna Estuary consists mostly of very fine sand and silt (Anwar and Rahman, 2021), whereas the suspended sediment typically consists of fine to medium silt near the water surface, silty sand at increasing depth, and sandy silt close to the bed (Borromeo et al., 2019). As would be

expected, coarser particles were moved by near-bed transport processes, whereas fine particles were predominantly transported as suspended material by the current. More than 70% of the suspended sediment in the upstream rivers had particle diameter smaller than 63 μm. Kuehl et al. (1989) observed that sediment in the estuary mainly comprised fine material. Borromeo et al. (2019) collected silt from the Bengal Shelf and found that particles of size < 5 μm occupied from 65 to 80% of the total sediment by weight at the locations considered. Barua (1990) reported that the turbidity maximum was generally located at or near the head of the salt intrusion where salinity is 1-5 ppt, and that its location fluctuated seasonally throughout the estuary.

One of the biggest challenges in studying the hydro-morphodynamic behaviour of the riverine and coastal system of Bangladesh is the unavailability of field data. Bricheno et al. (2016) mentioned Bangladesh as “notoriously data-poor” and reported that validation of a hydrodynamic model for this region is very difficult. Moreover, the quality of collected data is not good. Sediment data are scarce. During the field measurement campaign, data on suspended sediment data from Bangladesh Inland Water Transport Authority (BIWTA) were only obtained for 5 random days in 2007. By its very nature, sediment transport is a chaotic phenomenon depending on very complicated processes that are imprecisely understood. Even the best methods can calculate sediment transport rates to an accuracy of a factor of 2 in only 70% of cases in river engineering, and may not achieve accuracy of a factor of 5 in 70% of cases in coastal engineering (Soulsby, 1997).

Physical parameters and field data relevant to the floc size of suspended cohesive sediment in Meghna estuary are subject to considerable uncertainty. This in turn has a significant impact on estimates of sediment transport and morphological change. In practice, it is important to quantify such uncertainty and to understand how it affects the output parameters of hydro-morphological models, including sediment deposition and erosion. This paper describes use of the cohesive sediment transport version of Delft3D, an established hydro-morphological model, along with the numerical derived distribution approach to determine the propagation of uncertainty in floc size to uncertainty in sediment transport rate and bed morphological change at selected locations in the Meghna estuary, Bangladesh.

The paper aims to estimate uncertainty in sediment deposition rate at selected locations in the Meghna estuary, due to the underlying uncertainty in floc size (composed of 5 micron particles) using a numerical version of the derived distribution method. To the best of the authors’ knowledge, this is the first time the numerical derived distribution method has been applied to uncertainty in coastal

sediment transport processes. Here, we use a state-of-the-art, hydro-morphodynamic, regional-scale model to generate sediment transport scenarios in the Meghna Estuary and the Bay of Bengal. The paper is structured as follows. Section 2 compares different methods for assessing uncertainty propagation, provides a rationale as to why the numerical derived distribution approach is used herein, and describes the numerical derived distribution method used for uncertainty propagation. Section 3 outlines the Delft 3D hydro-morphodynamic model. Sections 4 and 5 respectively present and discuss the uncertainty propagation results. The main findings are listed in Section 6.

2. Uncertainty analysis and numerical derived distribution method

Uncertainty propagation analysis offers an effective theoretical means of assessing changes between distributions of input and output parameters at locations where field data are not easily available. Unknowns in physical parameters (i.e. parameter uncertainty), incomplete idealization of the physical processes, and model limitations (convergence, accuracy, and round-off errors) all contribute to uncertainty propagation. Initial and boundary conditions are routes by which uncertainty reaches the equation system. Examples include uncertainty in specification of bed friction roughness, sediment grain size, eddy diffusion coefficient, and other empirical closure parameters. The accuracy of outputs from a shallow flow water-sediment solver is therefore highly dependent on the accuracy of the input data. As indicated by Xiu (2009), it is important that uncertainty is taken seriously from the beginning of numerical model simulations in order to assess the reliability and possible variability of model outputs, which of course provide insight into the water-sediment processes. We will now very briefly comment on several of the more common methods used to assess uncertainty propagation.

Perhaps the earliest and simplest uncertainty assessment technique is sensitivity analysis whereby an input parameter is varied by ± per cent, and assessment made of the impact on an output variable. A typical example is the use of sensitivity analysis by Qin et al. (2002) to examine the effect of uncertainty in assigned weights and grades on the priority order of three options for post-reclamation coastline at Deep Bay, South China. Ni et al. (2002) used the assigned weights suggested by Qin et al. (2002) to determine an optimal reclaimed coastline from several options.

Stochastic modelling has been used for uncertainty quantification for more than a decade. Stochastic models estimate uncertainty propagation throughout the simulation, and are not limited to

calculating errors and bounds by post-processing the output (Lin et al., 2007). Horritt (2002) used first- and second-order perturbation methods to develop a stochastic model of shallow flow hydrodynamics, and thence to study the influence of uncertain bed topography. Horritt's stochastic model gave results in good agreement with Monte Carlo simulations. Flandoli and Pappalettera (2020) used a stochastic model to identify the noise required to reduce the complexity of interaction between different scales.

Monte Carlo simulation (and associated techniques) are routinely used to assess how the probability distribution of an input variable X translates into a probability distribution of an output variable Y (Hofer, 2018). Monte Carlo methods have been applied to uncertain flood prediction based on input parameter uncertainty using a simplified parameterization by Aronica et al. (1998) and Bates et al. (2004) and a distributed parameterization of a simplified model by Romanowicz and Beven (1998). Monte Carlo simulation is often used as a tool for risk assessment. For example, Lin and Schullman (2017) developed an integrated framework for risk assessment of cyclone-induced flooding, which considered storm climatology change, sea level rise and coastal development. Lin et al. used the Monte Carlo method to estimate risk metrics and the probability distribution of the present value of future losses. Wang and Wang (2019) created a high-resolution projection for Texas and produced a Markov chain Monte Carlo-based hydrologic forecast for the Guadalupe river basin. Xu et al. (2014) applied an integrated hydrodynamic model and Monte Carlo stochastic model of cyclone storm surges to predict extreme water levels in Colombo, Sri Lanka. In practice, Monte Carlo simulation is extremely useful, and can be readily extended to multiple input variable probability distributions. It does however suffer from a major shortcoming in that huge numbers (often > 10^5 or 10^6) of simulations are required as part of its repetitive resampling. This incurs an enormous computational overhead, rendering Monte Carlo unsuitable at present for application to complicated systems of nonlinear partial differential equations, such as the shallow water-sediment-morphodynamic equations considered in this article, given current computer technology. Moreover, it is difficult to assess the sensitivity of the results to the assumed input distributions, because a single change to an input distribution then requires re-running of the entire set of simulations. For the same reason, it is difficult to determine which input parameter has the greatest influence on output uncertainty using Monte Carlo simulation.

The derived distribution method used in our study is a faster approach than Monte Carlo simulation and has been widely applied in hydrological engineering. For example, by taking a first-order approximation of annual precipitation yield, Eagleson (1978) used the derived distribution approach to

determine the cumulative distribution function of annual yield from the cumulative distribution function of precipitation, and applied the approach to cases involving an arid climate (Santa Paula, California, USA) and a subhumid climate (Clinton, Massachusetts, USA). Díaz-Granados et al. (1984) obtained derived flood frequency distributions based on input distributions related to excess rainfall density, etc., for the Davidson, Santa Paula Creek, and Nashua River catchments in the USA. The derived distribution approach was applied to flood prediction in a basin in Italy comprising 16 poorly gauged watersheds (Brocchiola and Rosso, 2008). Chen and Adams (2007) used the derived distribution approach to develop an analytical stormwater quality model. Perona et al. (2013) obtained analytical expressions for probability distribution functions of optimally allocated river flows to human activity and the environment, using the derived distribution approach. Meier et al. (2016) estimated the probability distribution function of annual rainfall from short-term records and showed that the derived distribution approach can be used for datasets where information is missing in certain years.

Polynomial chaos methods greatly reduce or even remove the requirement of repetitive sampling that limits statistical sampling techniques like Monte Carlo simulation (Xiu, 2009). Polynomial chaos methods were first introduced in the early 2000s (Ghanem and Spanos, 2003; and Xiu and Hesthaven, 2005), and are very well documented in the literature (Xiu, 2010). The method can cope with a wide variety of stochastic variables, which represent the probability distribution function (Lacor and Savin, 2018). Polynomial chaos expansions have been applied in practical engineering problems, reducing the cost of computation in uncertainty quantification. However, the computational cost is still high when polynomial chaos is used for design optimization. Also, when information about the input probability distribution is incomplete, then the polynomial chaos expansion method may no longer be suitable.

It is obvious from the foregoing discussion that uncertainty propagation is a rapidly developing topic in data analytics. Of the methods considered, the derived distribution approach strikes a sensible compromise between accuracy and computational efficiency when applied to complicated model(s), and so is used herein. Herein, we adopt a numerical version of the derived distribution approach (following Kreitmair et al., 2019) to obtain the probability distribution of cohesive sediment deposition rate in the Meghna estuary. In the analytical version, both the independent and dependent variables are considered continuous, whereas in the numerical version, both are discrete.

In the analytical approach, the probability distribution function (PDF) of an input parameter is prescribed by an analytical expression wherein the standard deviation represents uncertainty in the input parameter. The cumulative distribution function (CDF) of the input parameter is obtained by integrating the PDF. The CDF of the output parameter is then determined by invoking conservation of probability and using the functional relationship between the input and output parameters. This is an efficient method to estimate uncertainty propagation, provided the functional relationship between input and output parameters is monotonic. The analytic version of the derived distribution method has been used to estimate parameter uncertainty for about fifty years. Ang and Tang (1975) demonstrated that the method can be adopted to determine the PDF of an output parameter directly from the PDF of an input parameter with the help of their monotonic functional relationship. All the higher moment statistics, such as skewness, kurtosis, etc. are then estimated. To the best of the authors' knowledge, the numerical version of derived distribution approach is applied herein for the first time to assess uncertainty in cohesive sediment deposition rate within a major tidal estuary.

A brief description of the concept behind the numerical derived distribution method now follows. According to Benjamin and Cornell (1970), "the likelihood that Y takes on a value on an interval of width $\mathrm{d}y$ centred on the value y is equal to the likelihood that X takes on a value in an interval centred on the corresponding value $x = g^{-1}(y)$ but of width $\mathrm{d}x = \mathrm{d}g^{-1}(y)$". Consider a parameter a that is assumed to be normally distributed with mean μ_a and standard deviation σ_a, such that.

$$N(a|\mu_a, \sigma_a^2) = \frac{1}{\sqrt{2\pi\sigma_a^2}} e^{\frac{(a-\mu_a)^2}{2\sigma_a^2}} \quad . \tag{1}$$

The corresponding cumulative distribution function is

$$\Phi(a|\mu_a, \sigma_a^2) = \frac{1}{\sqrt{2\pi\sigma_a^2}} \int_{-\infty}^{a_0} e^{\frac{(a'-\mu_a)^2}{2\sigma_a^2}} \mathrm{d}a'$$

$$= \frac{1}{2}\left[1 + \mathrm{erf}\left(\frac{a_0-\mu_a}{\sigma_a\sqrt{2}}\right)\right] \quad . \tag{2}$$

The probability that the value of a realization of random variable a falls between a_A and a_B, where $a_A < a_B$, is

$$\Pr(a_A < a < a_B) = \int_{a_A}^{a_B} N(a|\mu_a, \sigma_a^2)\, \mathrm{d}a$$

$$= \Phi(a_B) - \Phi(a_A)$$

$$= \frac{1}{2}\left[\mathrm{erf}\left(\frac{a_B-\mu_a}{\sigma_a\sqrt{2}}\right) - \mathrm{erf}\left(\frac{a_A-\mu_a}{\sigma_a\sqrt{2}}\right)\right] . \quad (3)$$

If the values of a are sufficiently finely spaced, then the likelihood of a value a_i being realised can be defined as the probability of a falling within the interval bounded by $a_{i-\frac{1}{2}}$ and $a_{i+\frac{1}{2}}$, such that

$$\Pr(a = a_i) = \Pr\left(a_{i-\frac{1}{2}} \leq a < a_{i+\frac{1}{2}}\right)$$

$$= \Pr\left(\frac{1}{2}\left(a_{i-\frac{1}{2}} + a_i\right) \leq a < \frac{1}{2}\left(a_i + a_{i+\frac{1}{2}}\right)\right)$$

$$= \frac{1}{2}\left[\mathrm{erf}\left(\frac{a_{i+\frac{1}{2}}-\mu_a}{\sigma_a\sqrt{2}}\right) - \mathrm{erf}\left(\frac{a_{i-\frac{1}{2}}-\mu_a}{\sigma_a\sqrt{2}}\right)\right] . \quad (4)$$

By analogy with the derived probability distribution, equation (4) also describes the associated probability of a maximum output value A, (e.g. of cohesive sediment transport rate) given that $A = f(a)$.

The expected value of A can be calculated as

$$E[A] = \sum_i A_i(a = a_i)\Pr(a = a_i), \quad (5)$$

and the variance is

$$\sigma_A^2 = \sum_i (A_i(a = a_i) - E[A])^2 \Pr(a = a_i) . \quad (6)$$

The higher order (n^{th}order) statistical moments are given by

$$\mu_n = \sum_i (A_i(a = a_i) - E[A])^n \Pr(a = a_i) , \quad (7)$$

where $n = 3$ provides the skewness of the distribution (indicating asymmetry) and $n = 4$ gives the kurtosis (indicating tailed-ness or peakedness).

The procedure for applying the numerical derived distribution approach is as follows:

i. Establish a functional relationship between the input parameter and output parameter from the simulated output. Plot the output parameter (u) against the input parameter (t). Use cubic spline to interpolate the values.

ii. Select a suitable standard probability distribution fitted to the mean and standard deviation of the input parameter data t. Then plot PDF $p(t)$ and CDF $c(t)$.

iv. Calculate the expected value $E[t]$ and variance $Var[t]$. These values should be such that $E[t]$~t and variance, $Var[t]$~σ_t^2.

v. Divide the PDF and CDF of t into a prescribed i number of bins. Determine the value of t at the middle of each bin. Then determine the corresponding values of u using the relationship between t and u.

vi. Determine the CDF values of t at both ends of each bin and find the corresponding values of t. The probability is the difference between these two values of u.

vii. Calculate the bin widths for u. These will be different from each other if the relationship between u and t is non-linear.

viii. Determine the PDF for u by dividing the probability of u of each bin by the width of the corresponding bin of u.

ix. Determine the CDF of u by numerical integration of the PDF of u.

x. Calculate expected value, variance, skewness and kurtosis of the output parameter using eqs 5, 6 and 7.

Fig. 2 gives a graphical representation of the principle behind the numerical derived distribution method.

3. Delft3D model set up

A two-dimensional depth averaged hydro-morphodynamic Delft3D model was established for the Bay of Bengal and coast of Bangladesh, which included sediment transport, entrainment, bed deposition and erosion processes. Figs 1 and 3 display the model domain and bathymetry. The model is based on a curvilinear grid with small cells (of 100+ m size) located in the estuary and large cells (up to 3400 m) in the bay. Use of small cell sizes in the estuary enabled generation of correct bathymetry and channel alignment in the region of interest, thus reducing computational error. Larger cells are located in the deep-water zone where the bathymetry is less complex. Riverbanks were modeled when generating the grid. Given that the coast of Bangladesh consists of multiple tributaries and islands, and its coastline has a rather fractal geometry, the model encompassed the entire coastline, including islands and tidal flats (allowing wetting and drying to occur).

The projected co-ordinate system adopted in the Delft3D model is the Bangladesh Transverse Mercator (BTM). Land elevation data were downloaded from the Earthexplorer webpage (https://earthexplorer.usgs.gov/) of the United States Geological Survey (USGS). These data were available in WGS84 geographic co-ordinate system, and then converted to BTM for input to the Delft3D model. The input bathymetry included measured bed elevations of rivers (data obtained from MorphoFlood project, IHE Delft, The Netherlands) and land elevations of islands (downloaded from the Earthexplorer website of the United States Geological Survey (USGS); https://earthexplorer.usgs.gov/). The depth-averaged version of Delft3D-FLOW software (Deltares, 2600 MH Delft, The Netherlands, https://oss.deltares.nl/web/delft3d) was used to simulate flow hydrodynamics and sediment transport in the Meghna estuary, and hence predict the sediment deposition rate. Using this approach, functional relationships were established between floc size and deposition rate at the locations of interest.

The model domain has two upstream open boundaries and one downstream open boundary, as indicated in Fig. 4. Constant river-discharges were prescribed at the two upstream boundaries. The Ganges-Brahmaputra river flow input was set to 120,000 m^3/s and the Meghna river flow was set as 20,000 m^3/s, representing the annual peak flood (data obtained from MorphoFlood project, IHE Delft, The Netherlands). The bathymetry for year 2007 obtained from the same project is also shown in Fig. 3. Following the tidal component input reduction method suggested by Latteux (1995), the downstream offshore boundary is tidal, comprising a single M_2 component (obtained from the TPXO 8.0 database using Delftdashboard tool from Deltares, The Netherlands; https://publicwiki.deltares.nl/display/DDB/Delft+Dashboard) multiplied by 1.20. This method utilizes a single representative tidal component rather than the whole set of tidal components in order to produce the same morphological changes in the long term. When validating the method, Latteux (1995) studied several locations in the vicinity of the English Channel, and represented the tidal behavior there using an equivalent single tide, finding that the representative tidal range was about 7 to 20% higher than the mean tidal range. However, the increase is case-specific, and depends on various parameters such as velocity, bathymetry, etc. In practice, a detailed investigation would be desirable to determine a value for the single representative tidal component for the Bay of Bengal, but in the absence of such information for the present hypothetical scenarios, it is assumed for simplicity that the representative tidal component is 20% higher than the actual M_2 component. The amplitude and phase are obtained from the TPXO 8.0 database using the DelftDashboard tool.

Manning's roughness parameter was used to describe bed friction in the Delft3D model. The procedure proposed by Soulsby (1997) and Whitehouse et al. (2000) was used to determine the spatial distribution of Manning's *n* . The bed shear stress is expressed as

$$\tau_0 = \rho u_*^2 \ , \tag{8}$$

where u_* is the friction velocity and ρ is density of water. The depth-averaged velocity is

$$\bar{u} = \frac{u_*}{\kappa}\left(\ln\frac{h}{z_0} - 1\right) , \tag{9}$$

where h is water depth (obtained from the model output), z_0 is bed roughness length and κ is the von Kármán constant (~0.4). The depth-averaged velocity was evaluated from the model output. The bed roughness length is calculated as

$$z_0 = \frac{k_s}{30}\left[1 - \exp\left(\frac{-u_* k_s}{27\nu}\right)\right] + \frac{\nu}{9u_*} \ , \tag{10}$$

where k_s is the Nikuradse roughness (= $2.5d_{50}$, in which d_{50} is the median particle diameter) and ν is the kinematic viscosity of water. Now, the friction velocity u_* is obtained by solving equations (9) and (10).

By definition, the bed shear stress is given by

$$\tau_0 = \rho C_D \bar{u}^2 \ , \tag{11}$$

and so,

$$\rho u_*^2 = \rho C_D \bar{u}^2 \ . \tag{12}$$

Then the drag coefficient can be calculated from

$$C_D = \left[\frac{\kappa}{\ln\frac{h}{z_0} - 1}\right]^2 \tag{13}$$

Also,

$$C_D = \frac{g}{C^2} \tag{14}$$

where C is the Chézy coefficient. Then,

$$C = \frac{R^{1/6}}{n} \tag{15}$$

where R is the hydraulic radius and n is Manning's parameter. For very wide channels, $R \approx h$, and so equation (15) can be written as,

$$n = \sqrt{C_D \frac{h^{1/3}}{g}} \ . \tag{16}$$

Fig. 4 shows the spatial map for Manning's parameter. The range of the value of Manning's n in Meghna estuary lies between 0.01-0.03 s/m$^{1/3}$.

In addition to water discharge, the open boundary of the Ganges-Brahmaputra river accommodates an extreme flood inflow of suspended sediment of concentration 0.799 kg/m^3. This value is based on the highest measured concentration of fine sediment at the open boundary, obtained on randomly selected days in 2007, 2008, and 2009 by the BIWTA. Sediment concentrations at the Meghna river boundary and the offshore boundary are assumed zero. The Meghna river has negligible morphological activity, and BIWTA has no data on suspended sediment concentration at this location. Turning to the offshore boundary it is assumed that no sediment enters the estuary from the deep ocean and all sediment reaching the bay from the river is deposited before reaching the offshore boundary.

Particle settling velocity is one of the most important parameters that influences sedimentation rate. Winterwerp and van Kesteren (2004) provide the following empirical expression for the settling velocity of fine sediment,

$$w_s = \frac{\alpha g}{18\beta\mu} \frac{\rho_s - \rho_w}{1 + .15 R_{ef}^{0.687}} d_p^{3-n_f} d_f^{n_f - 1} \ , \tag{17}$$

where d_p is particle diameter, d_f is floc diameter, R_{ef} is floc Reynolds number (given by $\frac{w_s d_f}{\nu}$, in which ν is kinematic viscosity of water), ρ_s is density of solid sediment, ρ_w is density of water, g is acceleration due to gravity, μ is fluid dynamic viscosity, α is a shape factor for gravitational force (which is equal to 1 for a spherical particle), β is a shape factor for drag force (which is equal to 1 for a spherical particle), and n_f = 3 for a Euclidean particle in the Stokes' regime where $R_e \ll 1$. Herein, the particle size of the

fine sediment is taken as 5 μm. The floc diameter is selected according to a probability distribution fitted to field data obtained by Winterwerp and van Kesteren (2004) who examined the relation between floc size and settling velocity of sediment obtained from several locations in the North Atlantic and North Sea, and noted that the floc diameter falls in the range of 20 μm – 1000 μm.

The critical bed shear stress for erosion in the case of fine sediment can be expressed as follows (Thorn and Parsons, 1980; Whitehouse et al., 2000):

$$\tau_e = E_1 {C_M}^{E_2} , \tag{18}$$

where τ_e is critical shear stress for erosion, C_M is dry density, and E_1 and E_2 are site-specific dimensional coefficients. E_1 is 5.42 × 10^{-6} for water-sediment samples of dry density between 30-200 kg/m^3 (Thorn and Parsons, 1980) and 0.0012 for water-sediment samples of dry density 30-400 kg/m^3 (Delo and Ockenden, 1992). Also, E_2 is 2.28 for water-sediment samples of dry density between 30-200 kg/m^3 (Thorn and Parsons, 1980) and 1.2 for water-sediment samples of dry density 30-400 kg/m^3 (Delo and Ockenden, 1992). Critical bed shear stress for deposition is typically half the value of the critical shear stress for erosion (τ_e). Laboratory tests have shown the critical bed shear stress for deposition to be about 0.06-0.10 N/m^2 (Whitehouse et al., 2000).

The Delft3D model was first run solely for hydrodynamics in the Meghna estuary, driven by tidal flow and river water discharge inputs. The simulation commenced from a cold start comprising an initial water level set 3 m vertically above mean sea level. After 7 days of hydrodynamic simulation, when the velocity and water level in the domain became stable, the output map file then provided the initial condition for the morphodynamic run. The time step of the model simulation was 0.5 minutes.

For the morphodynamic computations, one day of simulation time was set as the spin-up period, during which sediment transport calculations were undertaken without implementing bathymetry update. After spin-up, the duration of the morphodynamic change simulation was set to 14 cycles of the representative M_2 constituent tide, i.e. 7 days 5 hours and 50 minutes. In Delft3D, a morphological acceleration factor (Morfac) equal to 12 was used to optimize the model simulations of overall duration 3 months. It was important to run complete cycles of the tidal component while using Morfac because the hydrodynamic run-time was multiplied by Morfac to calculate morphological changes in Delft3D,

and so it was necessary to simulate complete tidal cycles in order to obtain the best possible output with less error. The time step for the morphodynamic change computations was 0.25 minutes.

4. Results

4.1 Model outputs

Before carrying out the computations, it was necessary to determine a suitable statistical distribution of floc sizes that might apply to the Meghna Estuary. In the absence of field data specific to the estuary, it was decided to use the extensive set of floc size data compiled by Winterwerp and van Kesteren (2004) from sites in the North Atlantic and North Sea. These floc size data were found to have a mean value of 227 μm and standard deviation of 171 μm. Several candidate probability distributions were then fitted to this data, and the chi-square (χ^2) goodness of fit test used to determine best fit distributions. Of the distributions considered, the Weibull and Gamma distributions gave the closest fits (Fig. 5). From the frequency distribution of floc size, χ^2 values $[\sum \frac{(Expected\ value - Observed\ value)^2}{Observed\ value}]$ were calculated for the Weibull and Gamma distributions. The χ^2 values for the Gamma and Weibull distributions were 696.2 and 719.1, respectively. Considering the significance level, α = 1%, the p-values for the Gamma and Weibull distributions were respectively 3.61×10^{-10} and 1.30×10^{-17}. Note that the p-value or the right-tail probability is the cumulative probability at $(1 - \chi^2)$ in the associated χ^2-distribution. If an assumed distribution has a p-value below the significance level, then the assumed distribution is acceptable. Hence, both Weibull and Gamma distributions proved to be suitable statistical representations of the floc size data. Given that the Gamma distribution had the smaller χ^2-value, the Gamma distribution was therefore selected as the best-fitted distribution for this case. This Gamma distribution has a mean of 227 μm, standard deviation of 169 μm (Fig. 5), and coefficient of variation of 169/227 ≈ 0.75.

Delft3D morphodynamic computations were then undertaken for six representative floc sizes: 20, 50, 100, 227, 500, and 1000 μm. Fig. 6 presents the sedimentation rate distribution in the Meghna estuary for flocs of different sizes, obtained from the simulation output. Smaller-sized flocs have lower settling velocities and hence exhibit lower deposition rates. The pattern of deposition of sediment indicates that deposition phenomena in the Meghna estuary are closely linked to its complicated

bathymetry, with erosion prevalent in the deeper reaches of rivers, and sedimentation evident in shallower areas (noting of course that the sediment deposition rate is driven by the combined effects of rivers and tidal current).

The erosion-deposition pattern along the estuary mouth is broadly similar to the historical map given by Brammer (2014). Both the map and model output indicate that the selected locations are prone to deposition. However, the model failed to generate erosion in the historically erosion-prone areas around Hatia and Sandwip islands. Furthermore, the model did not reproduce accretion along the whole Tetulia channel, illustrated in Brammer's map. There are several possible reasons for this. First, the model was not calibrated and validated against field observations for the sediment transport and bed morphodynamics calculations. Second, we assumed a constant single size of cohesive sediment particle and applied a constant single floc size throughout the domain in each simulation. In fact, the Meghna estuary contains particles and flocs that both have size distributions and are not single-valued. However, in the absence of field data on sediment particle and floc size distributions in the Meghna Estuary, and for model simplification purposes, the assumption was made bearing in mind that the aim of this paper is purely to look at uncertainty propagation. Even so, it must be emphasized that without proper information concerning the spatial variations in size distribution of particles in the Meghna estuary, the model outputs must be treated as purely hypothetical. Third, the model was run for a steady peak flood event lasting three months, representing a highly idealized extreme flood situation. Historical records show that such a prolonged extreme situation has not lasted for more than a week in the Meghna estuary. Fourth, it would have been computationally very expensive to simulate the morphodynamics over an entire monsoon season lasting 5-6 months, and so a simplified approach was taken using the morphological acceleration factor in the Delft3D simulation tool. Fifth, noting that the amount of erosion-accretion would be rather small during a short-duration peak flood event, a simulation time of 3 months was selected in order to drive obvious morphological change in the Bay of Bengal and around Meghna estuary. Of course, if the model input comprised more accurate time series of river flow, sediment size, and suspended sediment concentration covering the whole year including consecutive dry and monsoon seasons, then it would be expected that the model would produce output closer to historical evidence. Sixth, all the properties of the cohesive sediment were either assumed or calculated from theoretical formulae. The lack of field data about bed material, sediment size, unit weight, etc., are of course major sources of uncertainty. For reasons of brevity, this article focuses on

uncertainty arising from a single parameter, the floc size, and how it translates to uncertainty in sediment deposition/erosion rate.

Three locations, where the deposition rate is substantial, were selected for uncertainty analysis. Fig. 7 indicates the locations, which surround Bhola, the largest island of Bangladesh. Location 1 occupies a shallow area of West Shahbazpur channel at the northwest of Char Gazaria, where the mean depth is about 6 m (relative to mean sea level). Fig. 7 also shows the initial bathymetry, which corresponds to a complicated pattern of islands and shoals, created in the delta region as river branches meet the sea. The West Shahbazpur channel around this location is erosion prone, as confirmed by both the historical map and the Delft3D results. The depth-averaged velocity during high water is about 2.75 m/s and the current is invariably directed southward over the whole tidal cycle.

Accumulation of sediment occurs when and where flocs settle as the flow velocity slows. The flow direction reverses around the shallow tidal flats and islands during tidal high water, triggering the localized movement of sediment. Fig. 8 shows the local bathymetry (Fig. 8(a)) and the changes in sediment deposition/erosion per week averaged over 14 tidal cycles for increasing floc size (Fig. 8(b)-(g)). Fig. 8 indicates that the deposition-prone locations occur where the depth is predominantly shallow. It may also be seen that as the floc size increases, the deposition rate also increases. This occurs because the settling velocity increases progressively with increasing floc size, leading to more deposition of sediment.

Location 2 is a tidal flat in West Shahbazpur channel west of Manpura island. Fig. 9 depicts the initial bed condition and deposition after 14 cycles of M_2 tide (about a week). Fig. 9(a) shows the local bathymetry near Location 2, which is again characterized by islands and shoals. Again, deposition increases progressively with increase in floc size (Fig. 9(b)-(g)). Deposition is most prevalent in shallow areas where the flow velocity drops to zero or near-zero. The residual circulation adds to the deposition process by inducing further localized movement of sediment.

Location 3 is at the north of Bhola Kheyaghat in Tetulia channel. Fig. 10(a) shows the initial bed condition and Fig. 10(b)-(g) the bed morphology changes in the region of Location 3. Due to near-zero flow velocity during high water period, the Tetulia channel is deposition-prone. The river flow in Meghna follows the bathymetry in that the velocity is larger in the deeper channels. This results in erosion. Shallower areas display a depositional trend because of the low magnitude of flow velocity. Similar to previous cases, deposition increases as floc size increases because the settling velocity is proportional

to floc size, but the rate of increase becomes extremely low at the higher values of floc size (see Supplementary Information for 2-hourly velocity plots in a tidal cycle).

4.2 Convergence tests

The numerical uncertainty propagation method requires a response surface to be derived connecting values of the input parameter to the output response. Here, the morphodynamic version of Delft3D was used to predict output values of sediment deposition/erosion rate for a series of given input values of sediment floc size covering the majority of the range of floc sizes within the truncated probability distribution. Delft 3D was first run for floc sizes of 20, 50, 200, 500, 1000 microns, and the output sediment deposition/erosion rates in m/week extracted from the results at three locations of interest. To refine the parameter relationship between input floc size data and output sedimentation/erosion rate, a cubic spline was then fitted (using Matlab). Once the relationship was obtained, the uncertainty propagation method involved discretizing the probability density distribution for floc size into a number of bins, and then using the numerical derived distribution approach to determine the probability density distribution for sedimentation/erosion rate. It was important to conduct a convergence test to check that the probability density distribution had been divided into a sufficient number of bins.

Location 1, West Shahbazpur channel, northwest of Char Gazaria, Meghna estuary was selected as a suitable candidate site for the convergence test. Fig.11 shows the cubic spline that interpolates the functional relationship between (output) sedimentation rate and (input) floc size. As can be seen, this functional relationship is monotonically increasing. Fig. 12 shows the probability density distribution in floc size. The PDF exhibits strong asymmetry, with peak occurring at about 120 micron, and a long tail to 1000 micron.

Next, the statistical convergence of deposition rate is investigated according to the number of bins used to discretize the probability density function of floc size. Given that deposition rate is a function of floc size and that probability is conserved, the cumulative probability of a floc size is equal to the cumulative probability of the corresponding sedimentation rate. The transferred probability distribution contains the same number of bins, but the bin width is no longer fixed; this is because of the nonlinear

relationship between floc size and deposition rate (as obvious in Fig. 11). The numerical PDF transfer method is used to obtain the probability density of deposition rate and the statistical moments. Fig. 13 depicts the resulting probability density function and cumulative density function of deposition rate at Location 1 obtained for different numbers of bins used to discretize the probability density function of floc size. Table 1 summarizes the expected value and other statistical moments of sediment deposition rate at Location 1.

Table 1 indicates that the probability distribution of deposition rate is sensitive to the number of bins used to discretize the PDF of floc size. The expected value, variance, standard deviation and non-dimensional kurtosis of deposition rate converge to within two significant figures when the number of bins ≥ 400. Non-dimensional skewness converges to within one significant figure to a value close to zero. Consequently, the number of bins used in the following analysis is chosen as 400.

4.3 Uncertainty in model prediction of sediment deposition rate

Fig. 14 shows the relationships between sediment deposition rate and floc size, and the PDFs and CDFs at the three locations of interest. To be more specific, Fig. 14(d) and Fig. 14(g) display the PDF and CDF of sedimentation rate at Location 1. The peak of the derived probability distribution occurs at 0.16 m/week. The right-hand tail of the distribution appears elongated, a reflection of its asymmetry. The CDF approaches but does not quite reach unity. This slight mismatch would be expected to reduce if a larger number of bins were to be used for discretization and a larger portion of the stretched right-hand tail of the PDF taken into consideration. Table 2 lists the expected value, coefficient of variation, and other statistical moments of sediment deposition rate at Location 1. From Table 2, the expected value of the sedimentation rate at Location 1 is 0.22 m and the standard deviation is 0.0828 m. The coefficient of variation is smaller than unity, implying that this is a low-variant dataset. The non-dimensional skewness is ≈ 0, which indicates that the probability density distribution of sedimentation rate at Location 1 is almost symmetric around its mean. The kurtosis is a little below 3, which indicates that the probability density distribution of sedimentation at Location 1 is slightly flatter than a standard normal distribution. Propagation of uncertainty in floc size (75% of the mean value) caused the standard deviation of deposition rate to be 38% of the mean value. The coefficient of variation of deposition rate at Location 1 is smaller than that of the input floc size, implying the dispersion of the distribution of

deposition rate is less than that of floc size. Given that a high-variant distribution of floc size results in a low-variant distribution, the floc size of suspended particles of cohesive sediments does not seem to be a highly dominant parameter contributing to its deposition. The flow velocity, greatly influenced by the bottom geometry in this region, plays a vital role.

Fig. 14(e) and Fig. 14(h) show the PDF and CDF of deposition rate at Location 2. The peak of the derived probability distribution occurs for a deposition rate of 0.13 m/week. This PDF appears flatter than that of Location 1; i.e., the distribution is more dispersive. Table 2 summarizes the expected value and other statistical moments of sediment deposition rate at Location 2. Similar to Location 1, numerical data on the total deposition of sediment (in m) were obtained from the Delft3D results at Location 2, and the rate of deposition (in m/week) calculated. Next, a cubic spline was drawn connecting the resulting data on the rate of deposition of cohesive sediment (Fig. 14(b)). The same input probability density distribution of floc size as for Location 1 was utilized. From Table 2, the expected value of the sedimentation rate at Location 2 is 0.19 m and the standard deviation is 0.07 m. The coefficient of variation is less than 1 corresponding to a low-variant dataset. Non-dimensional skewness is negative, indicating that the tail of the probability density distribution is asymmetric; with most values leaning towards the left side of the mean value of deposition rate. Non-dimensional kurtosis is less than that at Location 1, and so this probability density distribution is flatter than the probability density of deposition rate at Location 1. The coefficient of variation of floc size is 75%, which is more than twice the coefficient of variation of deposition rate. The standard deviation, which indicates the uncertainty incorporated in a parameter, is 36% of the mean value of the deposition rate at Location 2. The derived probability distribution is less dispersed than the primary distribution of floc size, this is the similar trend as at location 1.

The PDF and CDF of deposition rate per week for Location 3 are shown in Fig. 14(f) and Fig. 14(i), derived from the PDF of floc size (Fig. 5) and the cubic spline drawn between deposition rate and floc size (Fig. 14(c)). The probability distribution reaches its peak for a deposition rate of 0.25 m/week. The left tail of this PDF is more elongated than the right tail. The CDF approaches close to 1. From Table 2, the expected value of sedimentation rate is 0.28 m and its standard deviation is 0.05 m, at Location 3. The coefficient of variation is 0.2, the lowest value among all three locations. Non-dimensional skewness is negative, which means the tail of the probability density distribution is asymmetric and the tail extends towards the left side of the mean value of the sedimentation rate.

Kurtosis is slightly higher than 3, which indicates that the probability density distribution of sedimentation rate at Location 3 is not as flat as a standard normal distribution. The probability density distribution here is even less variant than at the other locations; the input uncertainty in the floc size leads to an uncertainty of 20% in the mean value of the deposition rate.

5. Discussion

The foregoing results illustrate use of the numerical derived distribution method as a computationally efficient means of determining uncertainty in the sediment deposition rate of cohesive flocs at three point locations in the Meghna estuary. By means of hydro-morphodynamic simulations of hypothetical conditions in the estuary, it was found that the coefficient of variation reduced from 0.75 for input floc size to range from 0.2 to 0.38 for the sediment deposition rate at locations in West Shahbazpur channel and Tetulia channel, implying that the probability distribution of sediment deposition rate was less dispersed than that of the floc size. At all three locations, the flow depends on complicated local bathymetry, with sediment erosion/deposition strongly linked to local flow speed. Flocs deposit where the current speed, from combined river flow and tide, approaches zero. This is to be expected because as the flow stagnates, the particle settling velocity becomes an increasingly important driving parameter in sediment transport. Changes to bed morphology through local deposition and erosion processes, in turn affect the local flow field, leading to feedback between the hydrodynamics and morphology. In the regions of the Meghna estuary considered herein, we find shallow areas to be deposition-prone whereas deeper parts of the channels are erosion-prone. Of course, this is not a general observation for the whole estuary given that the analysis is restricted to just three point locations.

With shallower areas more prone to sediment deposition, nearby coastal areas are likely to experience higher flood risk as the estuary bed level increases. Deeper areas in the estuary, including some near the banks, are under threat of erosion. Partly because we considered a single cohesive sediment fraction size of 5 micron, our erosion-accretion patterns only partially match historical evidence given by Brammer (*2014*). Nevertheless, the model output shows that for all six floc sizes considered, significant deposition occurs at the mouth of the estuary. The smaller flocs cause less

sediment deposition whereas larger flocs cause heavier deposition (Fig. 6). Further investigations involving multiple sediment fractions are recommended to generate more realistic scenarios.

The numerical derived distribution method offers a very powerful tool by which to assess uncertainty propagation in hydro-morphodynamic models. Once sufficient model runs have been made in order to fit curves relating input to output parameters of interest, the method is remarkably fast and easy to apply. However, it does suffer from one drawback – the mathematical requirement that the input-output curves are monotonically increasing or decreasing owing to the unique nature of the mappings. This means that physical relationships involving turning points in input-output relationships cannot be treated using the derived distribution method to the authors' knowledge. Herein, the numerical derived distribution method was applied at three points of interest in the Meghna Estuary. In future, this analysis could be extended to provide contour maps of statistical parameters of uncertain input and output parameters by applying the derived distribution method to each grid point within the estuary. The present approach represents an initial step towards much more sophisticated analysis to come.

Estimates of the uncertain deposition rate can also be used to evaluate the changes to bed level elevation and hence flood risk at coastal areas in the Meghna estuary. Ongoing advances in decision-analysis under uncertainty (see e.g. Uusitalo et al., 2015; Simpson et al., 2016; Hodgett and Siraj, 2019; Bonjean Stanton and Roelich, 2021) offer systematic ways of managing flood risk for decadal to century-scale scenarios. The present study of uncertainty propagation from floc size to sediment deposition/erosion is important as it illustrates the application of an analysis support tool to a coastal region vulnerable to inundation. Such a tool could help develop coastal management strategies for Bangladesh, and incorporate climate change effects, such as uncertainty in sea level rise (using estimates for different Shared Socio-economic Pathways considered in the 6th Assessment Report by the Intergovernmental Panel on Climate Change) and human impacts. For example, the present analysis methodology could be useful in helping prioritise land reclamation options, thus aiding the coastal planning process in Bangladesh. For example, the Estuary Development Plan (*2007*) produced by the Ministry of Water Resources of Bangladesh identified several deposition-prone areas, for which uncertainty quantification could be highly beneficial. In areas where significant erosion may occur, uncertain erosion could be calculated as a precursor to assessing land erosion risk. The Intergovernmental Panel on Climate Change (IPCC) has stated that low lying countries like Bangladesh

will experience increased risk in flooding, salinization and erosion by the year 2100 (Openheimer et el., 2019), with the latest report stating that the whole of South Asia is under risk of severe shoreline retreat (Fox-Kemper et al., 2021). Erosion risk assessment will therefore help local authorities in Bangladesh plan long-term protective measures. Notably, the Bangladesh Delta Plan 2014 has adopted a holistic approach for which uncertainty quantification of key parameters related to relevant natural disasters would be extremely advantageous for agencies charged with coastal management and protection.

6. Conclusion

This article has investigated the use of the numerical derived distribution method to examine the effect of input uncertainty in floc size on output uncertainty in sediment deposition rate at three locations of interest in the Meghna estuary. The numerical derived distribution method proved to be very efficient, requiring very few full hydro-morphodynamic simulations. However, set against its speed and efficiency, the numerical derived distribution method is limited to cases where there is a unique mapping between input and output variables. The hydro-morphological model was quite simplified, being limited to cohesive suspended sediment under simplified tide and river flow driving conditions.

The application to three locations in the Meghna estuary revealed that uncertainty in deposition rate was relatively less sensitive to uncertainty in floc size, with values of normalized variance being lower for deposition rate than floc size. The probability density functions of sediment deposition rate ranged from almost symmetric platykurtic (i.e. fewer outliers than the normal distribution) in West Shahbazpur channel to left-skewed leptokurtic (i.e. more outliers than the normal distribution) at Bhola Kheyaghat. In a densely populated country like Bangladesh, land erosion is a threat to the supply of valuable land. Continuous deposition of suspended sediment near islands and narrow channels in the Meghna estuary increases the long-term flood risk to low lying coastal areas but also offers opportunities for land reclamation.

Future studies are required that investigate the deposition of different types and sizes of sediment in the Meghna estuary region. Field data on bed material and suspended sediment are vitally important as a prerequisite for accurate model predictions. Our paper offers a route towards more extensive studies of the morphological behavior of Meghna estuary considering other important parameters, such as multiple particle sizes of cohesive sediment based on field data, inclusion of non-cohesive sediment, bedload transport, salinity, tropical cyclones, Coriolis force, sea level rise, and

actual tide and river flow conditions. Such studies would be helpful to decision makers in planning flood mitigation measures, land protection works, and land reclamation activities. The numerical derived distribution approach has considerable potential as a tool for practitioners to estimate uncertain sediment transport, morphological change, and coastal risk arising from uncertainty in a wide range of different physical input parameters.

Acknowledgements

The first author is grateful to the Schlumberger Foundation Faculty for the Future Fellowship program for the financial support. The first author is also thankful to Prof. Alexander R. Horner-Devine for his help in Delft3D model development during the visiting program at The University of Washington, The USA, and to the Vest Scholarships for financing this visiting program. The bathymetry data and the river-discharge data were obtained from IHE Delft, The Netherlands and the authors are grateful to Prof. Dano Roelvink for sharing these data.

References

Akter, J., Sarker, M.H., Popescu, I., Roelvink, D., 2016. Evolution of the Bengal Delta and its prevailing processes. Journal of Coastal Research, 32(5), 1212–1226.

Allison, M.A., 1998. Historical changes in the Ganges-Brahmaputra delta. Journal of Coastal Research, 14(4), 1269-1275.

Ang, A. H-S., Tang, W. H., 1975. Probability concepts in engineering planning and design v.1: Basic principles. John Wiley and Sons, Inc., The USA.

Anwar, M.S., Rahman, K., 2021. The spatiotemporal shore morphological changes at east Bhola Island in Meghna Estuary of Bangladesh's central coast.Regional Studies in Marine Science, 47, 101937.

Aronica, G., Hankin, B., Beven K., 1998. Uncertainty and equifinality in calibrating distributed roughness coefficients in a flood propagation model with limited data. Advances in Water Resources, 22 (4), 349-365.

Bangladesh Planning Commission, 2018. Bangladesh Delta Plan 2100 Baseline Studies: Volume 1 - Water Resource Management. General economic Division, Bangladesh Planning Commission, Government of People's Republic of Bangladesh.

Barua, K.D., 1990. Suspended sediment movement in the estuary of Meghna river system. Marine Geology, 91, 243–253.

Barua, D.K., Kuehl, S.A., Miller, R.L., Moore, W.S., 1994. Suspended sediment distribution and residual transport in the coastal ocean off the Ganges-Brahmaputra river mouth. Marine Geology, 120, 41–61.

Barua, D.K., 1997. The active delta of the Ganges-Brahmaputra rivers: Dynamics of its present formations. Marine Geodesy, 20(1), 1-12.

Bates, P.D., Horritt, M.S., Aronica, G., Beven K., 2004. Bayesian updating of flood inundation likelihoods conditioned on flood extent data. Hydrological Processes, 18, 3347–3370.

Benjamin, J.R., Cornell, C.A.,1970. Probability, Statistics, and Decision for Civil Engineers,McGraw-Hill.

Bomer, E.J., Wilson, C.A., Hale, R.P., Hossain, A.N.M., Rahman, F.M.A., 2020. Surface elevation and sedimentation dynamics in the Ganges-Brahmaputra tidal delta plain, Bangladesh: Evidence for mangrove adaptation to human-induced tidal amplification. CATENA, 187, 104312.

Bonjean Stanton, M.C., Roelich K. 2021. Decision making under deep uncertainties: A review of the applicability of methods in practice. Technological Forecasting & Social Change, 171, 120939.

Borromeo, L., Ando, S., France-Lanord, C., Coletti, G., Hahn, A., Garzanti, E., 2019. Provenance of Bengal Shelf sediments: 1. Mineralogy and Geochemistry of silt. Minerals, MDPI, 9(10), 640.

Brammer, H., 2014. Bangladesh's dynamic coastal regions and sea-level rise. Climate Risk Management, 1, 51–62.

Bricheno, L. M., Wolf, J., Islam, S., 2016. Tidal intrusion with a mega delta: An unstructured grid modelling approach. Estuarine, Coastal and Shelf Science, 182, 12-26.

Brocchiola, D., Rosso, R., 2009. Use of a derived distribution approach for flood prediction in poorly gauged basins: A case study in Italy. Advances in Water Resources, 32(8), 1284-1296.

Chen, J., Adams, B.J., 2007. A derived probability distribution approach to stormwater quality modelling. Advances in Water Resources, 30(1), 80-100.

Delo, E.A., Ockenden, M.C., 1992. Estuarine muds manual. HR Wallingford Report SR 309.

Díaz-Granados, M.A., Valdes, J.B., Bras, R.L., 1984. A physically based flood frequency distribution. Water Resources Research, 20(7), 995-1002.

Eagleson, P.S.,1978. Climate, soil, and vegetation 7. A derived distribution of annual water yield. Water Resources Research, 14(5), 765–776.

Fischer, H.B., List, E.J., Koh, R.C.Y., Imberger, J., Brooks, N.A., 1979. Mixing in Inland and Coastal Waters. Academic Press Inc., New York.

Flandoli, F., Pappalettera, U., 2020. Stochastic modelling of small-scale perturbation, Water, 12(10), 1-17.

Fox-Kemper, B., H.T. Hewitt, C. Xiao, G. Aðalgeirsdóttir, S.S. Drijfhout, T.L. Edwards, N.R. Golledge, M. Hemer, R.E. Kopp, G. Krinner, A. Mix, D. Notz, S. Nowicki, I.S. Nurhati, L. Ruiz, J.-B. Sallée, A.B.A. Slangen, & Y. Yu, 2021. Ocean, Cryosphere and Sea Level Change. In Masson-Delmotte, V., P. Zhai, A. Pirani, S.L. Connors, C. Péan, S. Berger, N. Caud, Y. Chen, L. Goldfarb, M.I. Gomis, M. Huang, K. Leitzell, E. Lonnoy, J.B.R. Matthews, T.K. Maycock, T. Waterfield, O. Yelekçi, R. Yu, & B. Zhou (Eds.), Climate Change 2021: The Physical Science Basis. Contribution of Working Group I to the Sixth Assessment Report of the Intergovernmental Panel on Climate Change (pp. 1211–1362). Cambridge University Press. doi:10.1017/9781009157896.011.

Ghanem, R.G., Spanos, P.D., 2003. Stochastic finite elements: a spectral approach. Springer, New York.

Goodbred, S.L., Kuehl, S.A., 1999. Holocene and modern sediment budgets for the Ganges-Brahmaputra river system: evidence for highstand dispersal to flood-plain, shelf, and deep-sea depocenters. Geology, 27, 559–562.

Goodbred, S.L., Kuehl, S.A., 2000a.Enormous Ganges-Brahmaputra sediment discharge during strengthened early Holocene monsoon. Geology, 28(12), 1083–1086.

Goodbred, S.L., Kuehl, S.A., 2000b. The significance of large sediment supply, active tectonism, and eustasy on margin sequence development: late Quaternary stratigraphy and evolution of the Ganges-Brahmaputra delta. Sedimentary Geology, 133, 227–248.

Hodgett, R.E, Siraj, S. 2019. SURE: a method for decision-making under uncertainty. Expert Systems with Applications, 115, 684-694.

Hofer, E., 2018. The uncertainty analysis of model results, Springer, Cham.

Horritt, M.S., 2002. Stochastic Modelling of 1-D Shallow Water Flows over Uncertain Topography.Journal of Computational Physics, 180(1), 327-338.

Jakobsen, F., Azam, M.H., Kabir, M., 2002.Residual flow in the Meghna estuary on the coastline of Bangladesh. Estuarine, Coastal and Shelf Science, 55, 587–597.

Kabir, M.A., Salauddin, M., Hossain, K.T., Tanim, I.A., Saddam, M.M.H., Ahmad, A.U., 2020.Assessing the shoreline dynamics of Hatiya Island of Meghna estuary in Bangladesh using multiband satellite imageries and hydro-meteorological data.Regional Studies in Marine Science, 35, 101167.

Kreitmair, M. J., Draper, S., Borthwick, A. G. L., van den Bremer, T. S., 2019. The effect of uncertain bottom friction on estimates of tidal current power.Royal Society Open Science, 6, 180941.

Kuehl, S.A., Hariu, T.M., Moore, W.S., 1989. Shelf sedimentation off the Ganges–Brahmaputra river system: Evidence for sediment bypassing to the Bengal fan. Geology, 17, 1132–1135.

Lacor C., Savin É., 2019. General Introduction to Polynomial Chaos and Collocation Methods. In: Hirsch C., Wunsch D., Szumbarski J., Łaniewski-Wołłk Ł., Pons-Prats J. (eds) Uncertainty Management for Robust Industrial Design in Aeronautics. Notes on Numerical Fluid Mechanics and Multidisciplinary Design, vol 140. Springer, Cham.

Latteux, B., 1995. Techniques for long-term morphological simulation under tidal action. Marine Geology, 126, 129-141.

Lin, G., Wan, X., Su, C., Karniadakis, G. E., 2007. Stochastic computational fluid mechanics. Computing in Science & Engineering, 9 (2), 21-29.

Lin, N., and Shullman, E., 2017. Dealing with hurricane surge flooding in a changing environment: part I. Risk assessment considering storm climatology change, sea level rise, and coastal development. Stochastic Environmental Research and Risk Assessment, 31, 2379–2400.

Mahmood, R., Ahmed, N., Zhang, L., Li, G., 2020. Coastal vulnerability assessment of Meghna estuary of Bangladesh using integrated geospatial techniques. International Journal of Risk Reduction, 42, 1-14.

Meier, C. I., Moraga, J. S., Pranzini, G., Molnar, P., 2016. Describing the interannual variability of precipitation with the derived distribution approach: effects of record length and resolution, Hydrology and Earth System Sciences, 20, 4177-4190.

Mikhailov, V.N., Dotsenko, M.A., 2007. Processes of delta formation in the mouth area of the Ganges and Brahmaputra rivers. Water Resources, 34, 385–400.

Milliman, J.D., Meade, R.H., 1983.World-wide delivery of river sediments to the oceans. Journal of Geology, 91, 1-22.

Mukherjee, A., Fryar, A.E., Thomas, W.A., 2009. Geologic, geomorphic and hydrologic framework and evolution of the Bengal basin, India and Bangladesh. Journal of Asian Earth Sciences, 34, 227-244.

Ni, J.R., Borthwick, A.G.L., Qin, H.P., 2002. ‘‘Integrated approach to determining postreclamation coastlines.’’ Journal of Environmental Engineering, 128(6), 543–551.

Oppenheimer, M., B.C. Glavovic , J. Hinkel, R. van de Wal, A.K. Magnan, A. Abd-Elgawad, R. Cai, M. Cifuentes-Jara, R.M. DeConto, T. Ghosh, J. Hay, F. Isla, B. Marzeion, B. Meyssignac, & Z. Sebesvari, 2019. Sea Level Rise and Implications for Low-Lying Islands, Coasts and Communities. In H.-O. Pörtner, D.C. Roberts, V. Masson-Delmotte, P. Zhai, M. Tignor, E. Poloczanska, K. Mintenbeck, A. Alegría, M. Nicolai, A. Okem, J. Petzold, B. Rama, N.M. Weyer (Eds.), IPCC Special Report on the Ocean and Cryosphere in a Changing Climate (pp. 321–445). Cambridge University Press. https://doi.org/10.1017/9781009157964.006

Perona, P., Durrenmatt, D.J., Characklis, G.W., 2013. Obtaining natural-like flow releases in diverted river reaches. Journal of Environmental Management, 118, 161-169.

Qin, H.P., Ni. J.R., Borthwick, A.G.L., 2002. Harmonized optimal postreclamation coastline for Deep Bay, China. ASCE Journal of Environmental Engineering, 128(6), 552-561.

Rogers, K.G., Goodbred, S.L., Mondal, D.R., 2013. Monsoon sedimentation on the ‘abandoned’ tide-influenced Ganges-Brahmaputra delta plain. Estuarine, Coastal and Shelf Science 131, 297–309.

Romanowicz, R., Beven, K., 1998. Dynamic real-time prediction of flood inundation probabilities. Hydrological Sciences Journal, 43(2), 181-196.

Sarker, M.H., Huque, I., Alam, M., 2003.Rivers, chars and char dwellers of Bangladesh. International Journal of River Basin Management, 1, 61–80

Seijger, C., Datta., D. K., Douvena, W., van Halsemac, G., Khan, M.F., 2019. Rethinking sediments, tidal rivers and delta livelihoods: tidal river management as a strategic innovation in Bangladesh. Water Policy, 21, 108–126.

Siddique-E-Akbar, A.H.M., Hossain, F., Lee, H., Shum, C.K., 2011. Inter-comparison study of water level estimates derived from hydrodynamic–hydrologic model and satellite altimetry for a complex deltaic environment. Remote Sensing of Environment, 115(6), 1522-1531.

Simpson, M., James, R., Hall, J.W., Borgomeo, E., Ives M.C., Almeida, S., Kingsborough, A., Economou, T., Stephenson, D., Wagener T., 2016. Decision Analysis for Management of Natural Hazards. Annual Review of Environment and Resources, 41, 489–516.

Soulsby, R., 1997. Dynamics of marine sands: A manual for practical applications. Thomas Telford Publications, London.

Thorn, M.F.C., Parsons, J.G., 1980. Erosion of cohesive sediments in estuaries: an engineering guide. 3rd International Symposium of Dredging Technology, Bordeaux, 349-358. BHRA, Cranfield, U.K.

Uusitalo, L., Lehikoinen, A., Helle, I., Myrberg, K., 2015. An overview of methods to evaluate uncertainty of deterministic models in decision support. Environmental Modelling & Software, 63, 24-31.

Wang, S., Wang, Y., 2019. Improving probabilistic hydroclimatic projections through high-resolution convection-permitting climate modeling and Markov chain Monte Carlo simulations. Climate Dynamics, 53, 1613–1636.

Whitehouse, R., Soulsby, R., Roberts, W., Mitchener, H., 2000. Dynamics of estuarine muds: A manual for practical applications. Thomas Telford Publications, London.

Winterwerp, J. C., van Kesteren, W. G. M., 2004. Introduction to the physics of cohesive sediment in the marine environment. Development in Sedimentology 56, Elsevier, Amsterdam.

Xiu, D., Hesthaven, J.S., 2005. High-order collocation methods for differential equations with random inputs, SIAM Journal on Scientific Computing, 27(3), 1118-1139.

Xiu, D., 2009. Fast numerical methods for stochastic computations: a review. Communication in Computational Physics, 5(2-4), 242-272.

Xiu, D., 2010. Numerical methods for stochastic computations. Princeton University Press, Princeton, USA, 2010.

Xu, S., Huang, W., Zhang, G., Gao, F., Li, X., 2014. Integrating Monte Carlo and hydrodynamic models for estimating extreme water levels by storm surge in Colombo, Sri Lanka. Natural Hazards, 71, 703–721.

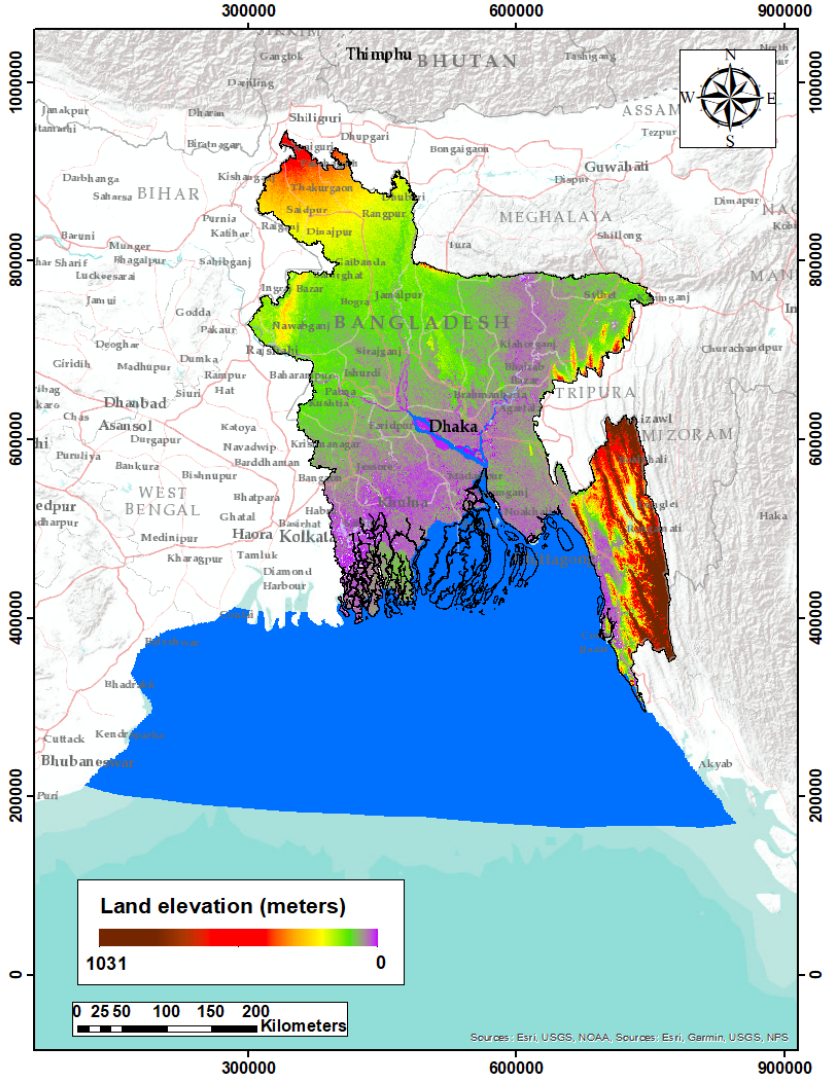

Fig. 1.Map showing land elevation of Bangladesh (data downloaded from https://earthexplorer.usgs.gov/). The Delft3D model domain is shown in blue. The geographic boundary of Bangladesh was downloaded from www.geodash.gov.bd.

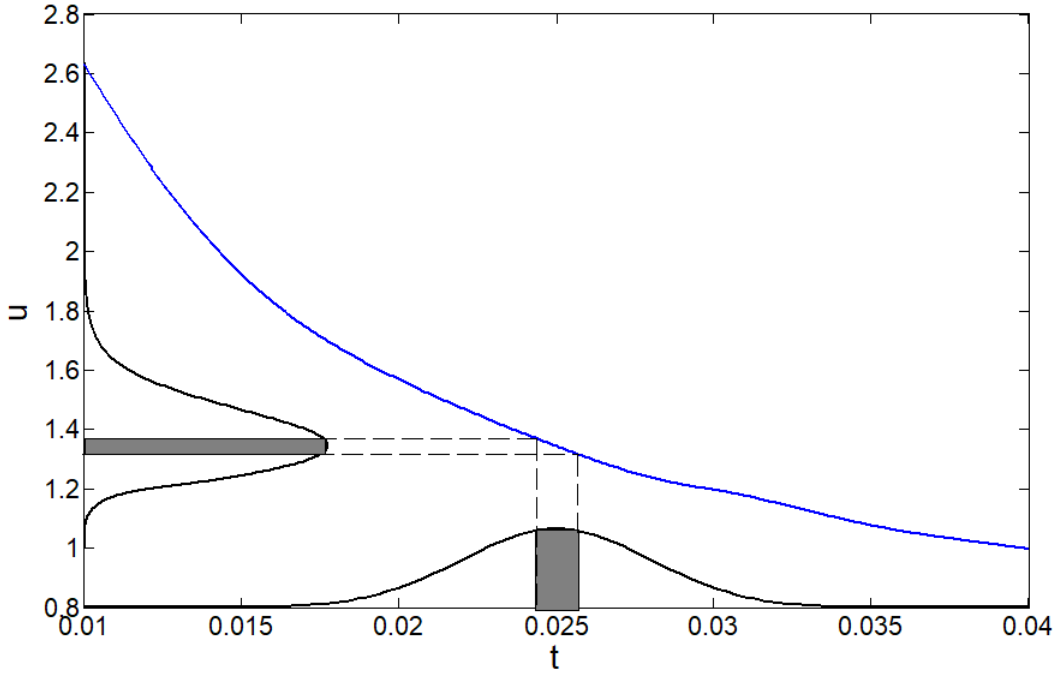

Fig. 2: Principle of derived distribution method where the PDF of u is derived from the PDF of t and the simulated relationship between them.

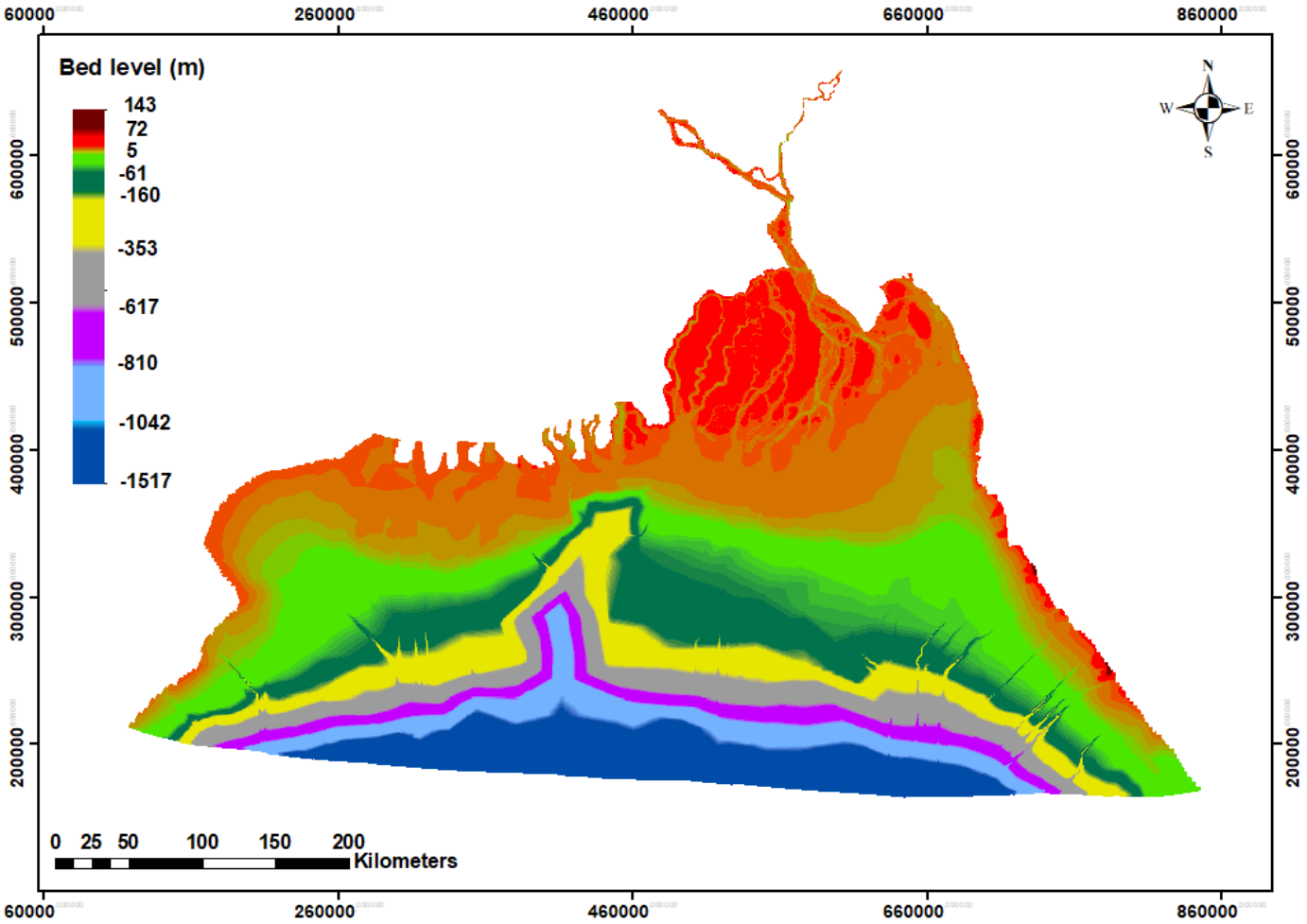

Fig. 3: Model bathymetry. River bed levels (data obtained from MorphoFlood project, IHE Delft, The Netherlands) and island land elevations (downloaded from https://earthexplorer.usgs.gov/) within the Delft3D domain for the Meghna estuary and Bay of Bengal.

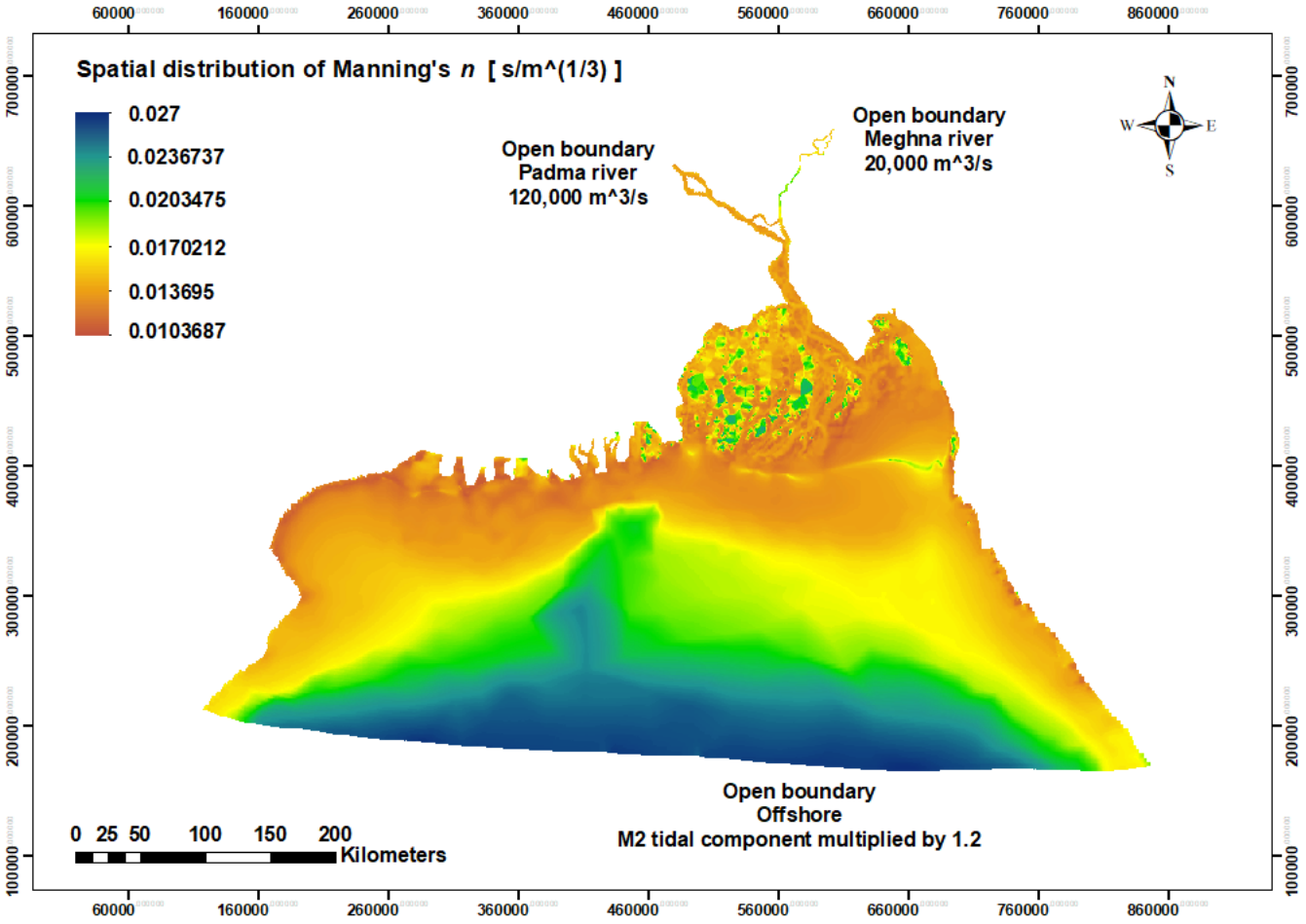

Fig. 4: Spatial map of Manning's n for the Meghna estuary domain, generated using the procedure by Soulsby (1997) and Whitehouse et al. (2000). Open boundary conditions are also shown.

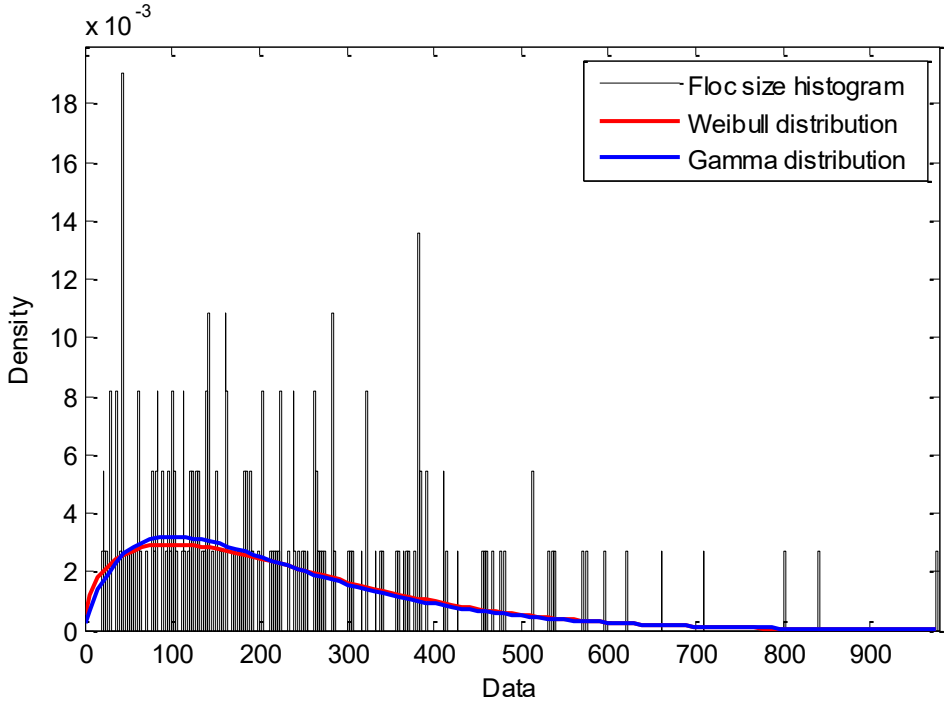

Fig. 5: Floc size data from Winterwerp and van Kesteren (2004) classified in 480 bins with fitted Gamma and Weibull distributions superimposed.

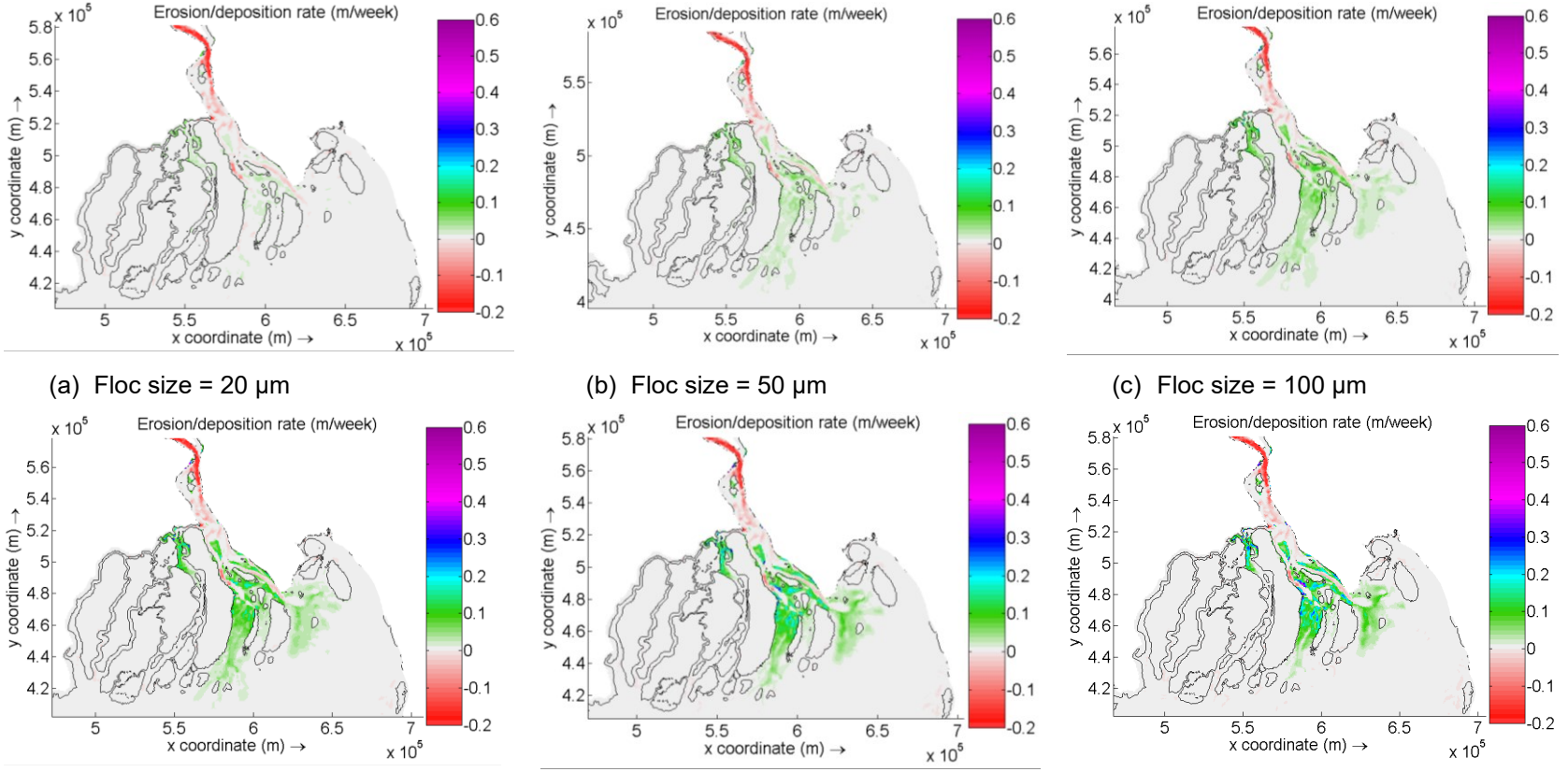

(a) Floc size = 20 μm (b) Floc size = 50 μm (c) Floc size = 100 μm

(d) Floc size = 227 μm (e) Floc size = 500 μm (f) Floc size = 1000 μm

Fig. 6: Spatial distribution of cohesive sediment deposition rate (m/week) in Meghna estuary after 14 cycles of 1.2 M_2 constituent tide for different floc sizes.

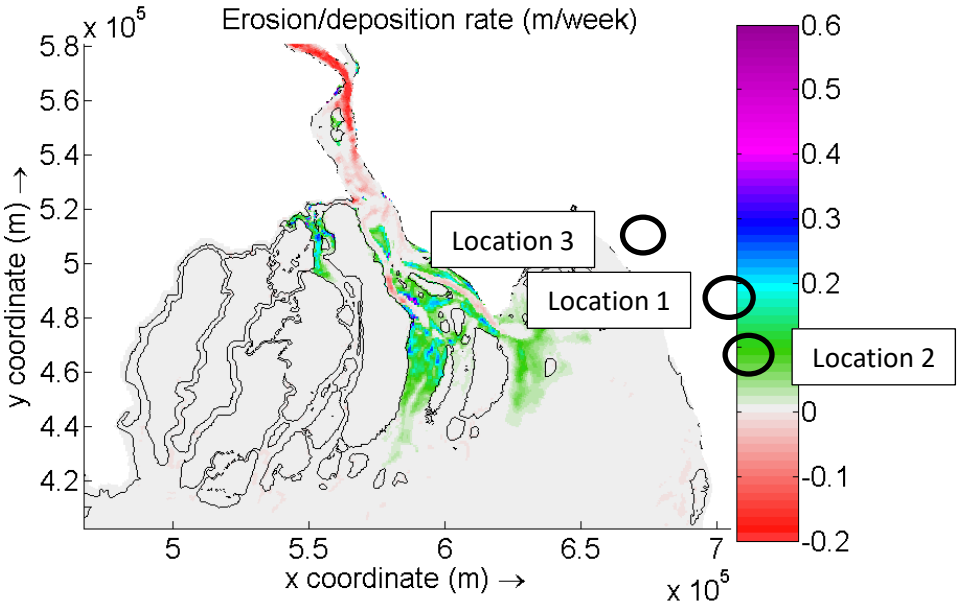

Fig.7: Locations considered in uncertainty analysis of sediment transport rate in Meghna estuary, Bangladesh: Location 1 is in West Shahbazpur channel, northwest of Char Gazaria; Location 2 is in West Shahbazpur channel west of Manpura island; and Location 3 is north of Bhola Kheyaghat in Tetulia channel.

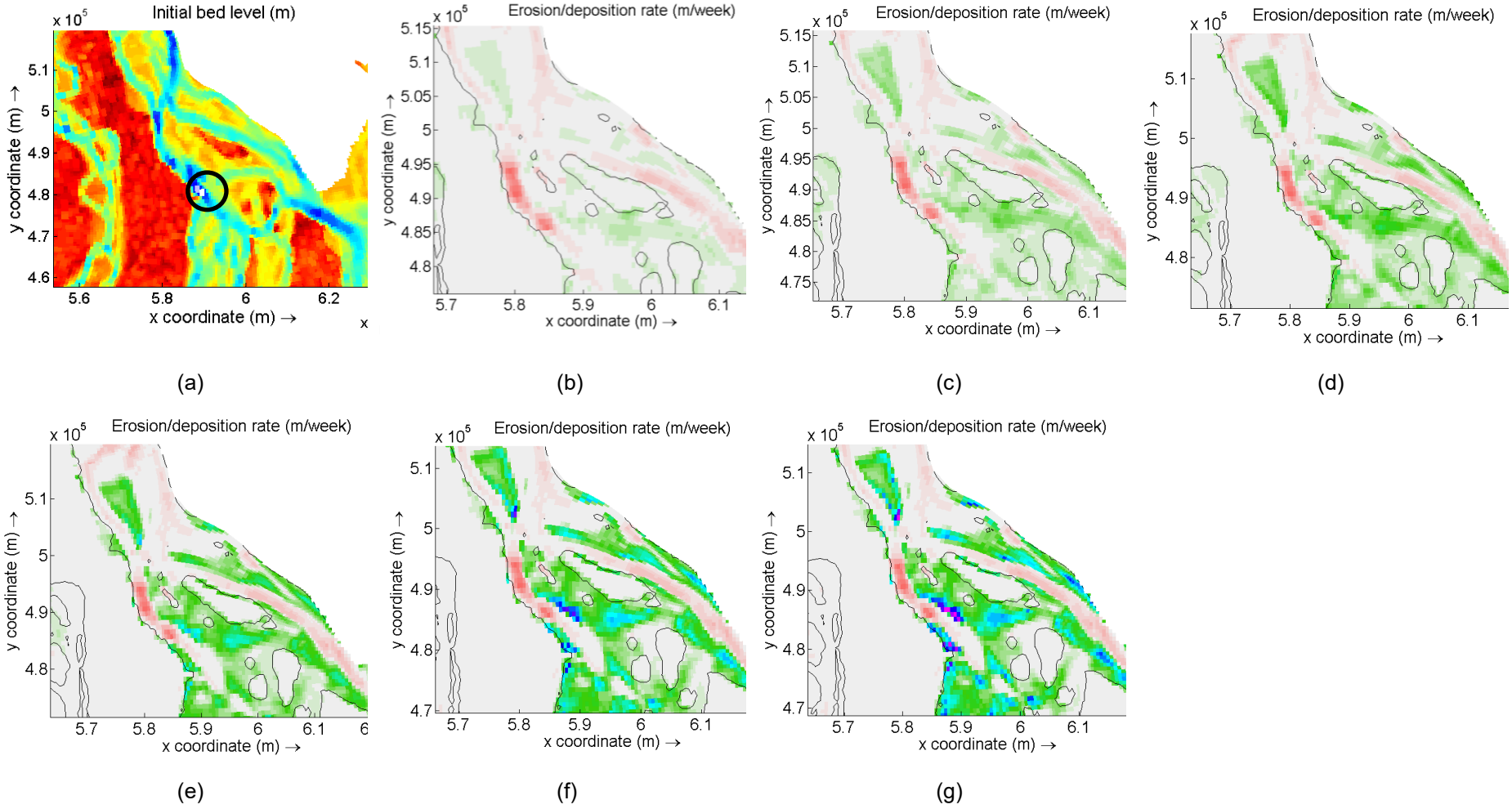

Fig. 8: (a) Initial bed level in vicinity of Location 1 (black circle), West Shahbazpur channel,northwest of Char Gazaria, Meghna estuary. Erosion and accretion obtained by considering 14 cycles of the 1.2 M_2 constituent tide for the following floc sizes: (b) 20 μm, (c) 50 μm, (d) 100 μm, (e) 227.21 μm, (f) 500 μm, and (g) 1000 μm.

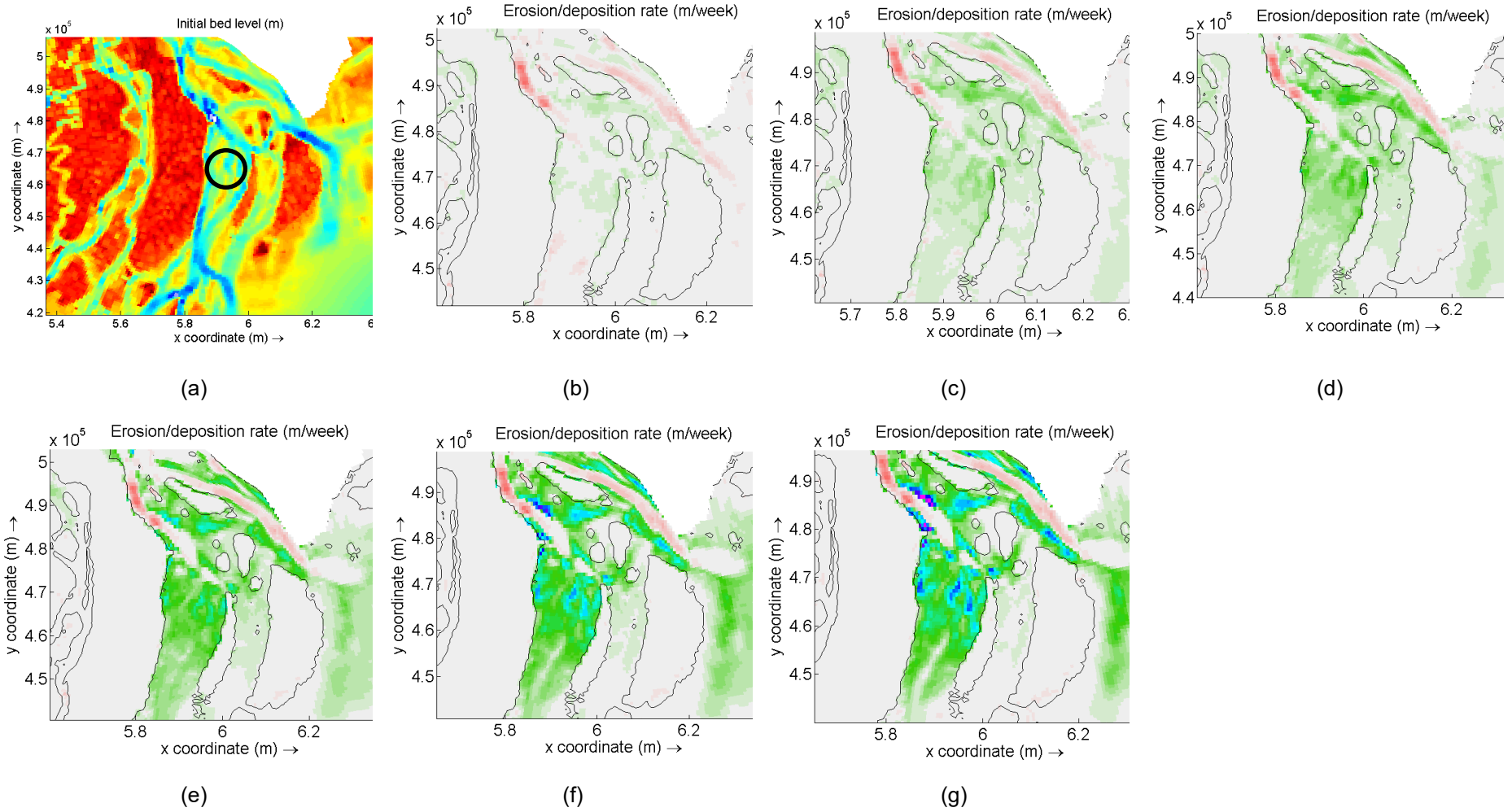

Fig. 9: (a) Initial bed level in vicinity of Location 2, West Shahbazpur channel, west of Manpura island, Meghna estuary. Erosion and accretion obtained by considering 14 cycles of the 1.2 M_2 constituent tide for the following floc sizes: (b) 20 μm, (c) 50 μm, (d) 100 μm, (e) 227.21 μm, (f) 500 μm, and (g) 1000 μm.

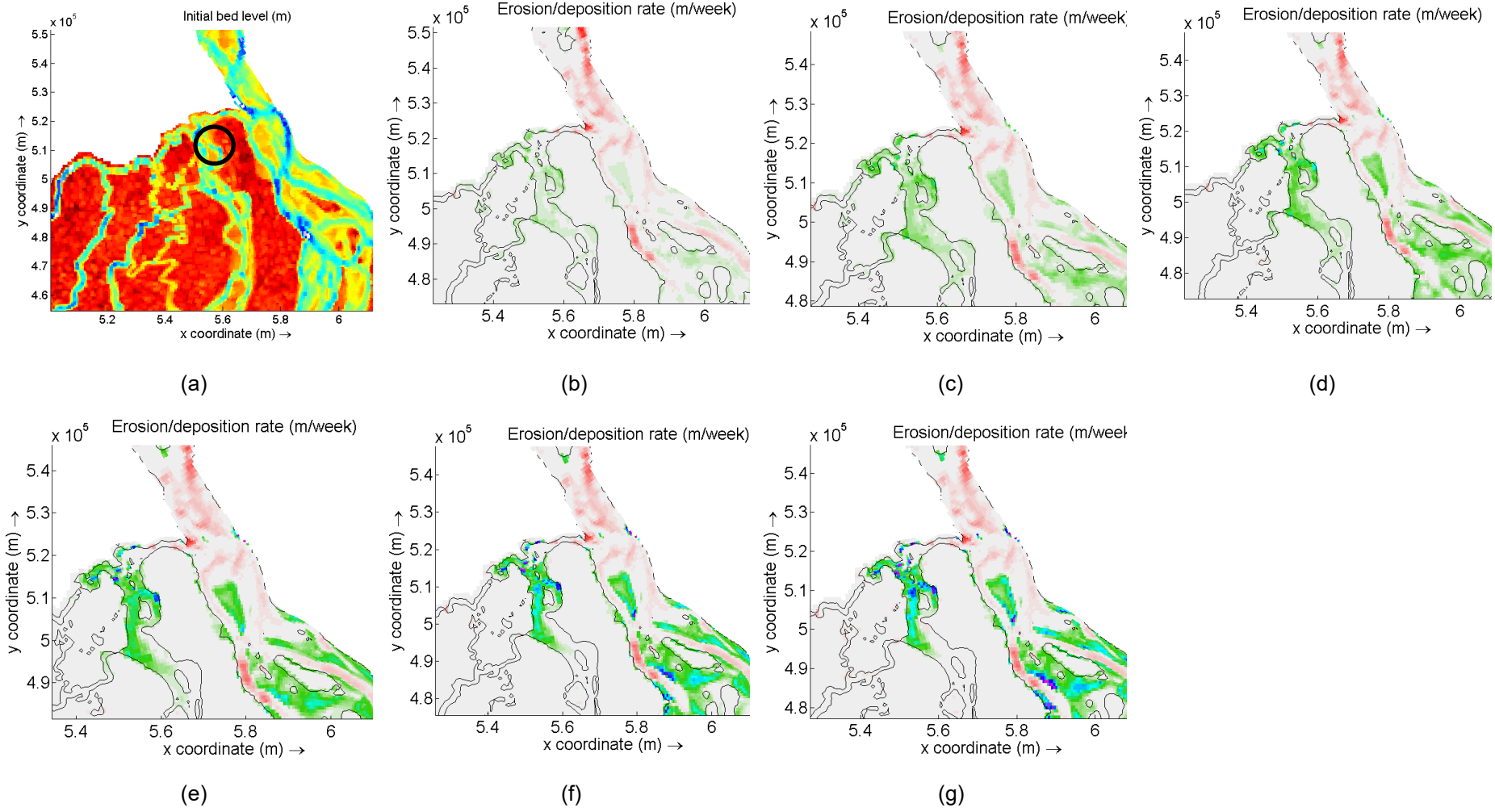

Fig. 10: (a) Initial bed level in vicinity of Location 3, north of Bhola Kheyaghat, Tetulia channel, Meghna estuary. Erosion and accretion obtained by considering 14 cycles of the 1.2 M_2 constituent tide for the following floc sizes: (b) 20 μm, (c) 50 μm, (d) 100 μm, (e) 227.21 μm, (f) 500 μm, and (g) 1000 μm.

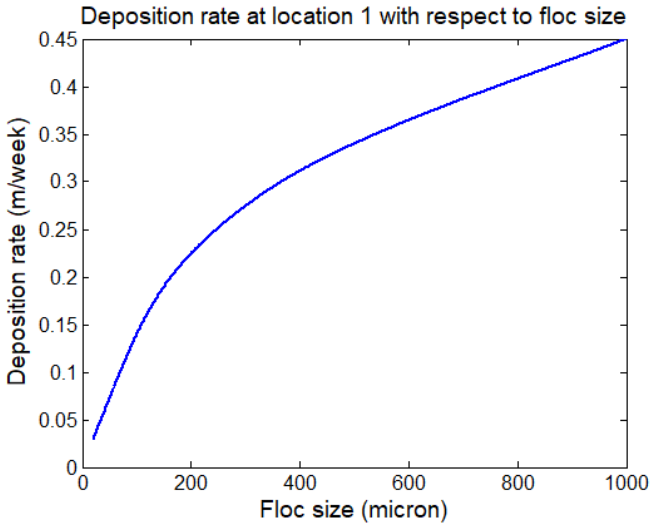

Fig. 11: Cubic spline relation between sedimentation rate and floc size at Location 1, West Shahbazpur channel, northwest of Char Gazaria, Meghna estuary, obtained by considering 14 cycles of the 1.2 M_2 constituent tide.

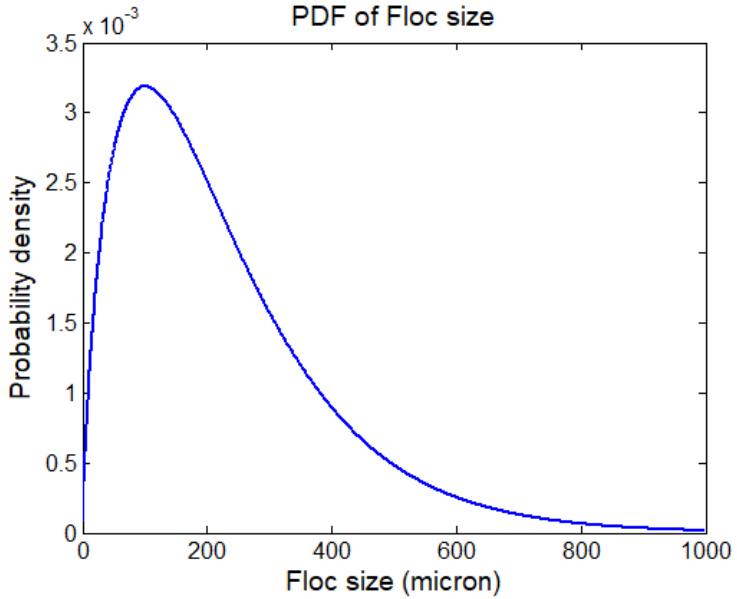

Fig. 12: Probability density function of floc size of cohesive sediment at Location 1, West Shahbazpur channel, northwest of Char Gazaria, Meghna estuary, obtained from data given by Winterwerp and van Kesteren (2004).

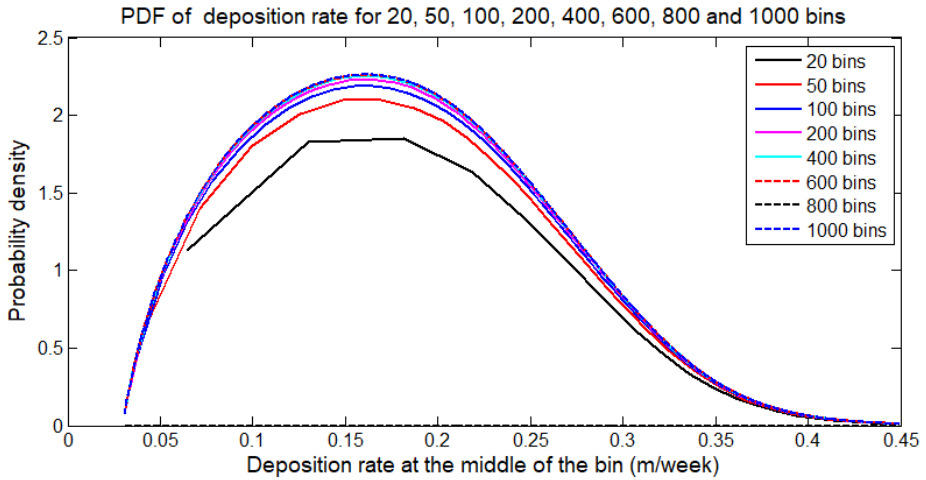

(a)

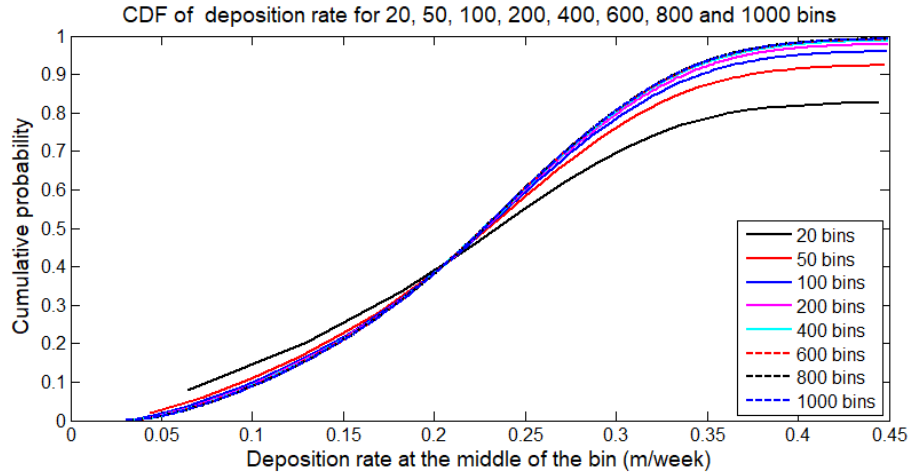

(b)

Fig. 13: PDF (a) and CDF (b) of sedimentation rate at Location 1, West Shahbazpur channel, northwest of Char Gazaria, Meghna estuary, plotted for different numbers of bins, obtained by considering 14 cycles of the 1.2 M_2 constituent tide.

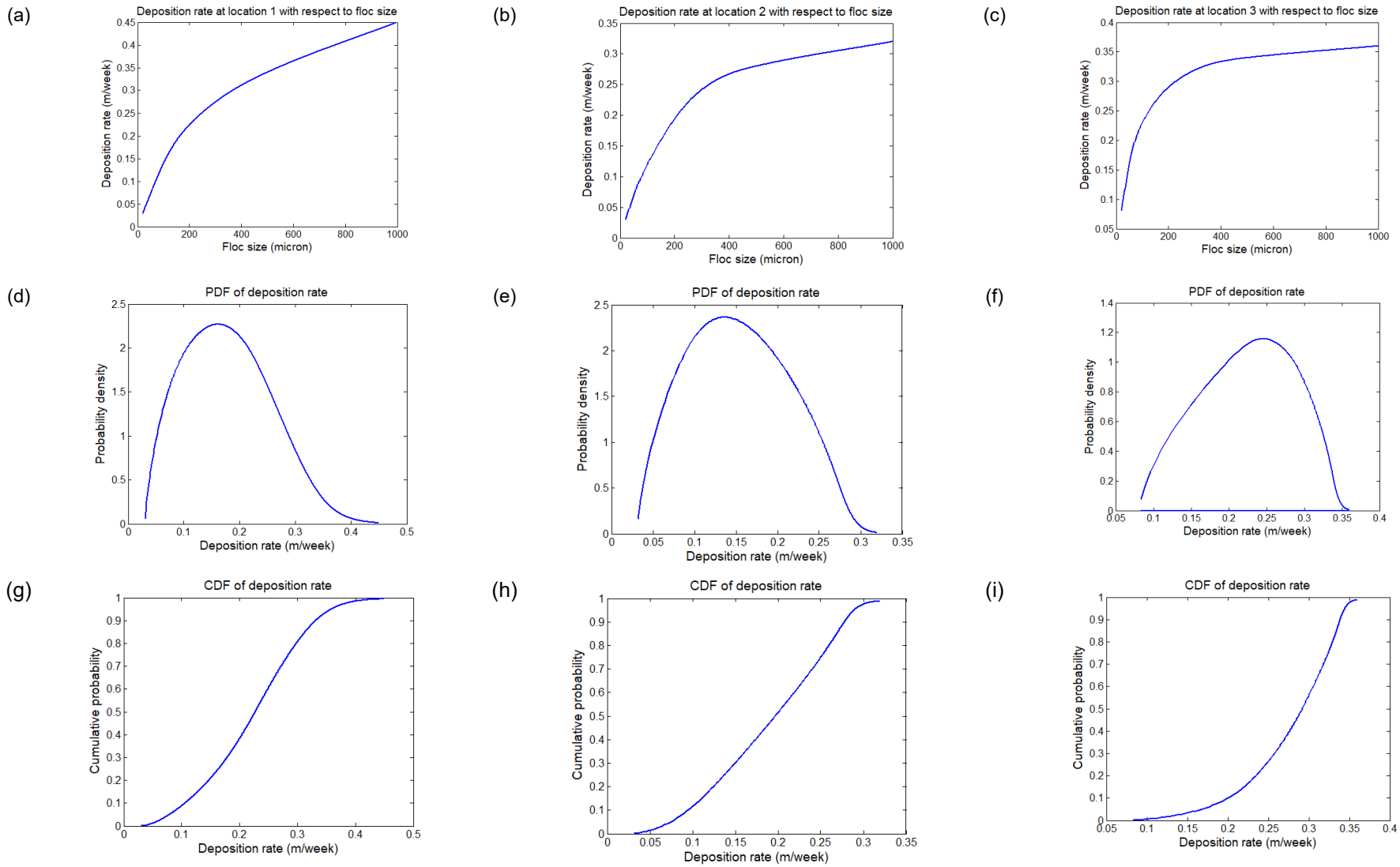

Fig. 14: Floc size and sediment deposition in the Meghna estuary. The first row (a-c) shows cubic spline fits between sediment deposition rate and floc size at Locations 1, 2, and 3. The second (d-f) and third rows (g-i) depict PDFs and CDFs of deposition rate at the same locations, obtained by considering 14 cycles of the 1.2 M_2 constituent tide.

Table 1: Expected value and other statistical moments of sedimentation rate at Location 1,West Shahbazpur channel, northwest of Char Gazaria, Meghna estuary.

No. of bins	Expected value of deposition rate, $E[D]$ (m/week)	Variance, σ_D^2 (m^2/week^2)	Standard deviation, σ_D (m/week)	Non-dimensional skewness, $Skew_n(D)$	Non-dimensional kurtosis, $Kurt_n(D)$
20	0.1818	0.0072	0.0848	1.1318	2.9149
50	0.2052	0.0067	0.0821	0.5257	2.6053
100	0.2135	0.0068	0.0822	0.2453	2.5079
200	0.2178	0.0068	0.0826	0.0992	2.4654
400	0.2200	0.0069	0.0828	0.0219	2.4463
600	0.2207	0.0069	0.0830	-0.0041	2.4403
800	0.2211	0.0069	0.0830	-0.0172	2.4374

Table 2: Expected value and other statistical moments of sediment deposition rates at Locations1, 2 and 3 in the Meghna estuary.

Location	Mean floc size (μm)	Expected value of deposition rate, $E[D]$ (m/week)	Standard deviation, σ_D (m/week)	Coefficient of variation, $\frac{\sigma_D}{E[D]}$	Non- dimensional skewness, $Skew_n(D)$	Non- dimensional kurtosis, $Kurt_n(D)$
1	227	0.22	0.08	0.38	0.0219	2.4463
2	227	0.19	0.07	0.36	-0.1567	2.0362
3	227	0.28	0.05	0.2	-0.7917	3.3127